TABLE OF CONTENTS

LIST OF TABLES

Page

LIST OF FIGURES

Page

LIST OF ABBREVIATIONS

3D	Three-dimensional
AA	Aluminum Alloy
Bi	Biot number
CAD	Computer Aided Design
FE	Finite Element
FEA	Finite Element Analysis
HSBF	High Speed Blow Forming
HTC	Heat Transfer Coefficient
IR	Infra-red
PID	Proportional Integral Derivative
QPF	Quick Plastic Forming
SP	Super Plastic
SPF	Super Plastic Forming
TC	Thermocouple

LIST OF SYMBOLS

Symbol	Description	Unit
A	Surface area	m^2
c (C_p)	Specific heat capacity	J/Kg^{o}C
C	Constant	-
g	Gravity acceleration	N/Kg
h	Convective heat transfer coefficient	W/m^2C
h_f	Forced convective heat transfer coefficient	W/m^2C
h_n	Natural convective heat transfer coefficient	W/m^2C
H	Dimension	m
k	Conductive heat transfer coefficient	W/m^{o}C
K	Constant	-
l	Characteristic length	m
L	Dimension	m
m	Mass	Kg
n	Constant	-
Nu	Nusselt number	-
Pr	Prandtl number	-
q	Heat energy	J
$\dot{q}$	Heat transfer rate	W
Ra	Rayleigh number	-
S	Surface area	m^2
T_1, T_2	Temperature in time t_1, t_2	^{o}C
$\dot{T}$	Temperature variation rate	^{o}C/s

T_s	Surface temperature	ºC
T_∞	Ambient temperature	ºC
x, y, z	Coordinates	-
β	Thermal expansion coefficient	1/ºK
ε	Emissivity	-
$\dot{\varepsilon}$	Strain rate	s^{-1}
v	kinematic viscosity	m^2/s
σ	Stress	N/m^2

INTRODUCTION

Nowadays using aluminum and aluminum alloys has been vastly expanded. Light weight, recyclability, workability and corrosion resistance are among the advantages of this metal that has made it more widely used. Because of the low weight to strength ratio, it has become a preferable material for weight saving purposes in the transportation industries. Extrusion, rolling, sheet metal forming, stamping, die casting, and forging are the conventional manufacturing methods of aluminum products (Davis, 1993; Kaufman, 2000). Beside the common mentioned methods, Super Plastic Forming (SPF) is a specific method of production that could be used for some alloys of aluminum. Superplasticity is a characteristic of a material, which allows applying large strains in a tensile condition before failure. As some of the aluminum alloys show the superplastic behavior, then it is possible to produce them with the SPF method. SPF is an advanced manufacturing method that allows forming very complex shapes in one action, which is not possible by the conventional stamping method. In this method with applying gas pressure at high temperature, the superplastic sheet material is formed into the SPF die. Transportation industries (land, sea, and aerospace) utilize this technique for the production of high value added components. High production cycle time, due to the low deformation rate, is the major challenge of this method which is not favorable for mass production scale industries such as automotive sector. In recent years, there have been many efforts to overcome the above problem and High Speed Blow Forming (HSBF) also known as Quick Plastic Forming (QPF) has been introduced as an alternative method that allows the use of higher strain rate in comparison with the conventional SPF (Gillo Giuliano, 2011; Majidi, Jahazi, & Bombardier, 2018b, 2019). HSBF is based on the SPF and the technical challenges of the both techniques are almost the same.

Verbom Inc. is a Canadian base company that utilizes both techniques for the production of body panels for electric cars and trains. This project has been defined with the collaboration of Verbom to experimentally and numerically investigate the temperature variation during the entire SPF/HSBF process and consider the distortion issue as one of the important problems

of the SPF/HSBF products. This work was practically divided into three main sections and the results of each section have been presented as a paper and shown in the frame of a chapter.

This thesis has been structured in four chapters. In chapter 1, introducing the SPF and HSBF process, effective parameters and technical challenges during the process, objectives of the work, and literature review are presented. Chapter 2 presents the experimental and numerical investigation of the temperature evolution in a HSBF tool during the preheating stage of the process with the view to minimize the duration of the preheating stage and obtain more uniform temperature distribution on the HSBF die at the end of the process. In chapter 3, the temperature evolution within a SPF part during the cooling stage of the SPF process has been numerically and experimentally analyzed. In the final chapter, the distortion issue of the SPF part as a function of the cooling stage after the end of the forming stage is investigated.

CHAPTER 1

LITERATURE REVIEW

1.1 Super Plastic Forming (SPF)

Superplasticity is the capability of a material to undergo large uniform strains, sometimes more than 1000 %, prior to failure under tensile loading conditions. Fig. 1.1 shows a superplastic titanium alloy with a high elongation. SPF is an advanced manufacturing process, which is able to form a superplastic sheet metallic material to very complex geometries in one operation.

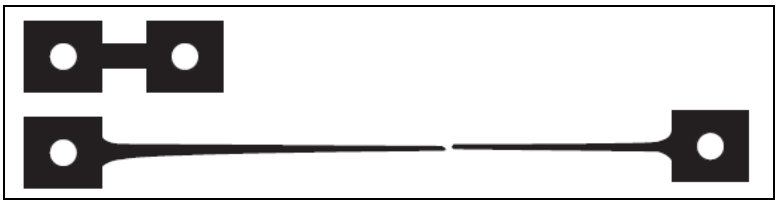

Figure 1-1 Super plastic titanium alloy before and after deformation (Gillo Giuliano, 2011)

The SPF process is carried out with the pressure of an inert gas at the back of the SPF sheet metal. The inert gas is blown onto the sheet metal and shapes it into the SPF die cavity. The characteristics of the SPF process are low strain rate ($<10^{-3}$ S^{-1}), high temperature (>0.5 T_m), small grain size (between 5 and 15 μm), and high strain rate sensitivity (>0.3). The SPF method is widely used in aerospace industry and in recent years it has been applied in the ground transportation industries. The flow stress-strain rate relation in the SPF process can be expressed by the equation below.

$$\sigma = K\dot{\varepsilon}^m \tag{1.1}$$

The low strain rate in the SPF process is a disadvantage that restricts the application of the method in the mass production industries like automotive. AA5083, AA2004, AA7475, AA2090, and AA8090 are some SP aluminum alloys, which are of industrial interest (Gillo

Giuliano, 2011; Guo, 2005; Majidi et al., 2019). Fig. 1.2 shows some SPF products made of AA7475 for the aerospace industry.

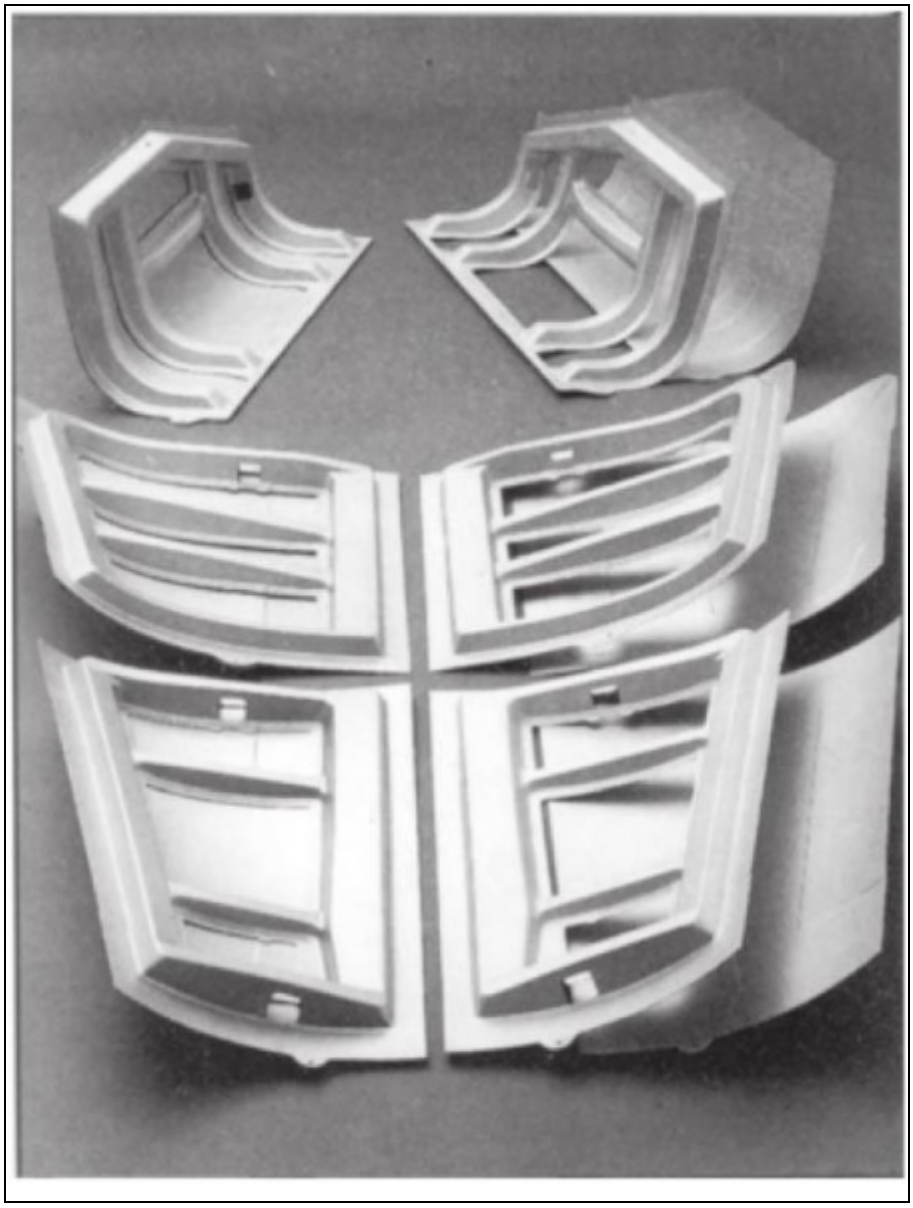

Figure 1-2 SP components made of AA7475 (Guo, 2005)

SPF tool usually consists of two heating platens with the source of heating and two dies i.e. lower and upper. For the sake of energy saving, depending on the design, usually there are some insulators around the SPF tool. In the first step of the SPF process, the dies should reach

to the target temperature as the forming temperature of the SPF part, in this regard, the tool is usually heated up in an offline mode (out of press) which sometimes takes more than 25 hours depending on the size of the tool. After reaching to the target temperature, the tool is installed on the press. For performing the forming process, the part must also reach to the target temperature. This heating process could be done out of the installed tool or inside of it between the dies. After the heating process, the dies are completely closed and the pressure of the inert gas is applied in a defined manner to control the strain rate. Pressure of the gas form the blank sheet into the SPF die and at the end, the pressure is discharged. Then, the die is opened for the ejecting process. The cooling step starts from the instant the part is ejected on a carrier that brings it outside of the forming press where the part is cooled to room temperature through natural convection or using blowing fans. Fig. 1.3 illustrates schematically different steps of a SPF process.

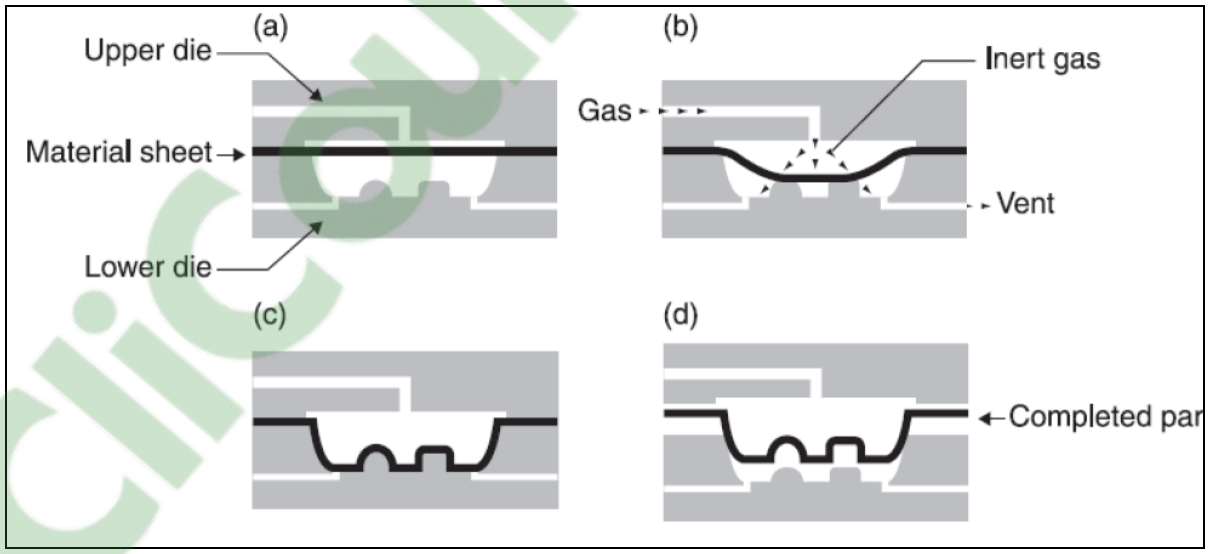

Figure 1-3 The schematic of a SPF process a) closing the die, b) blow forming, c) shape part, d) ejecting (Gillo Giuliano, 2011)

1.2 High Speed Blow Forming (HSBF)

As mentioned above the major challenge of the SPF process is the low strain rate or high production cycle time, which makes it as non-economic method for the mass production scale. In this regard, significant efforts have been made for the compensation of the issue, and as a result, HSBF known as QPF as well, has been recently introduced. Both techniques exploit pre mechanical deformation of the sheet material before the blow forming process with considerably higher strain rate (up to 10^{-1} s^{-1}). In the HSBF method, usually the forming die and sometimes a simple punch preforms (crash forms) the sheet material and then the blowing process shapes the part to the final form. Fig. 1.4 depicts the schematic of a HSBF process.

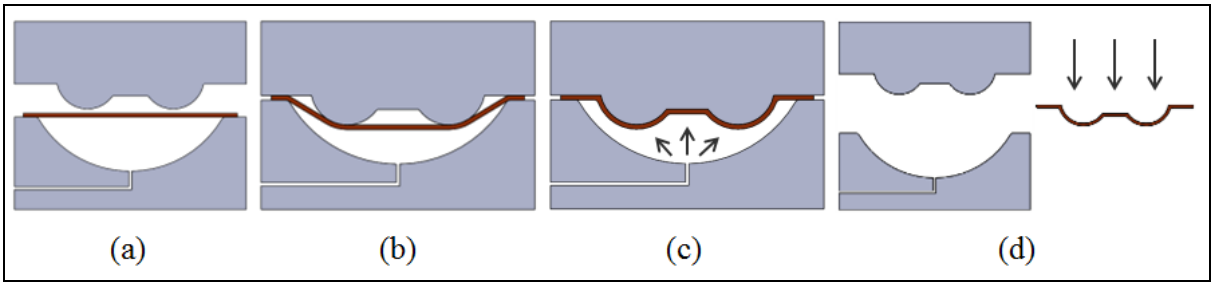

Figure 1-4 The schematic of a HSBF process a) heating the sheet material, b) preforming, c) blow forming, d) cooling

The differences between the SPF and HSBF have been shown in table 1.1 and Fig. 1.5 shows a production line of a HSBF process. More detailed discussions are also available in (Boissiere, Terzi, Blandin, & Salvo, 2008).

Table 1-1 The differences between the SPF and HSBF process (Gillo Giuliano, 2011)

Superplastic forming process	Quick Plastic Forming process
Forming rates/temperatures chosen to exploit maximum material ductility	**Forming rates/temperatures chosen to maximize productivity consistent with final quality**
Aerospace market • Lower-volume (100s of panels/year) • High-price-point products • Hand re-work common for dimensional and surface quality	**Automotive markets** • Higher-volume (tens of 1000s panels/year) • Low-price-point products (consumer goods) • Emphasize first-time dimensional and surface quality
Manufacturing system • Low level of automation, manual handling • Low capital, high piece cost	**Manufacturing system** • High level of automation, robotic handling • Higher investment, lower piece cost
Typical SPF panels • Extreme shapes • High forming strains – back pressure to limit cavitation • Maximum mechanical properties (including 2XXX, 7XXX alloys)	**Typical QPF panels** • Moderate shapes (but more complex than automotive metal stamping) • Moderate forming strains – back pressure not required • Moderate post-form properties (primarily 5XXX alloys)
Niche process	**High-volume process**

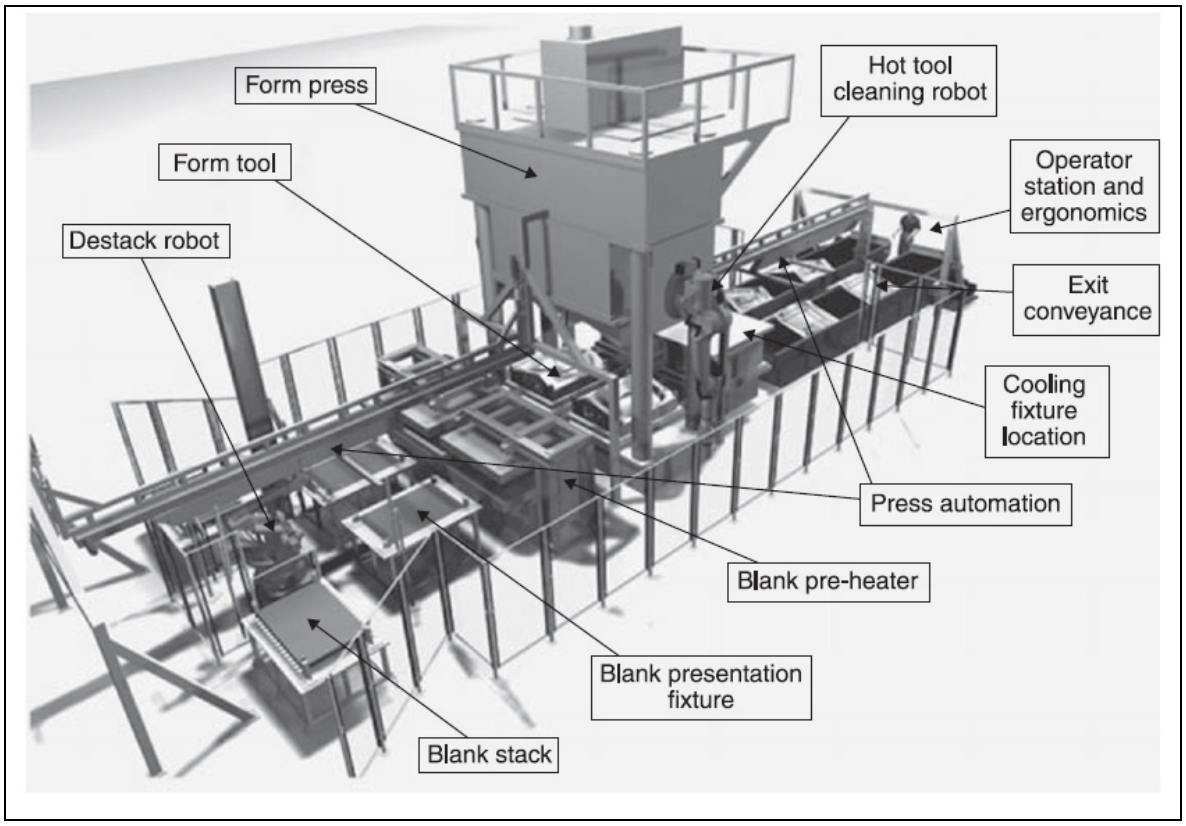

Figure 1-5 A production line of a HSBF process (Gillo Giuliano, 2011)

1.3 Problematic and challenges in SPF/HSBF of aluminum alloy sheet

The important parameters that affect the quality of the final product in the SPF/HSBF process are as below:

a) Temperature;
b) Strain rate;
c) Strain rate sensitivity;
d) Friction;
e) Grain size;
f) Geometry of the component;

Lack of control or optimization of the above parameters could lead to galling, cavitation, wrinkling, distortion, and even fracture of the part. Among the above defects, distortion is one

of the most frequent ones that result in part rework and extra costs. Therefore, it is of critical importance to better understand the origins of the distortion with the view to minimize its occurrence. The main objective of the present thesis is to study the thermal aspects of the SPF/HSBF process with particular attention on the impact of the heating and cooling process in the final distortion of the part.

1.4 Heat transfer and temperature evolution during the SPF/HSBF process

During the SPF/HSBF process, both mechanical and thermal phenomena occur and affect the tool and the part. For the heating of the tool, usually heating elements are installed on the heating platens or inside the dies. Fig. 1.6 shows each case of installation.

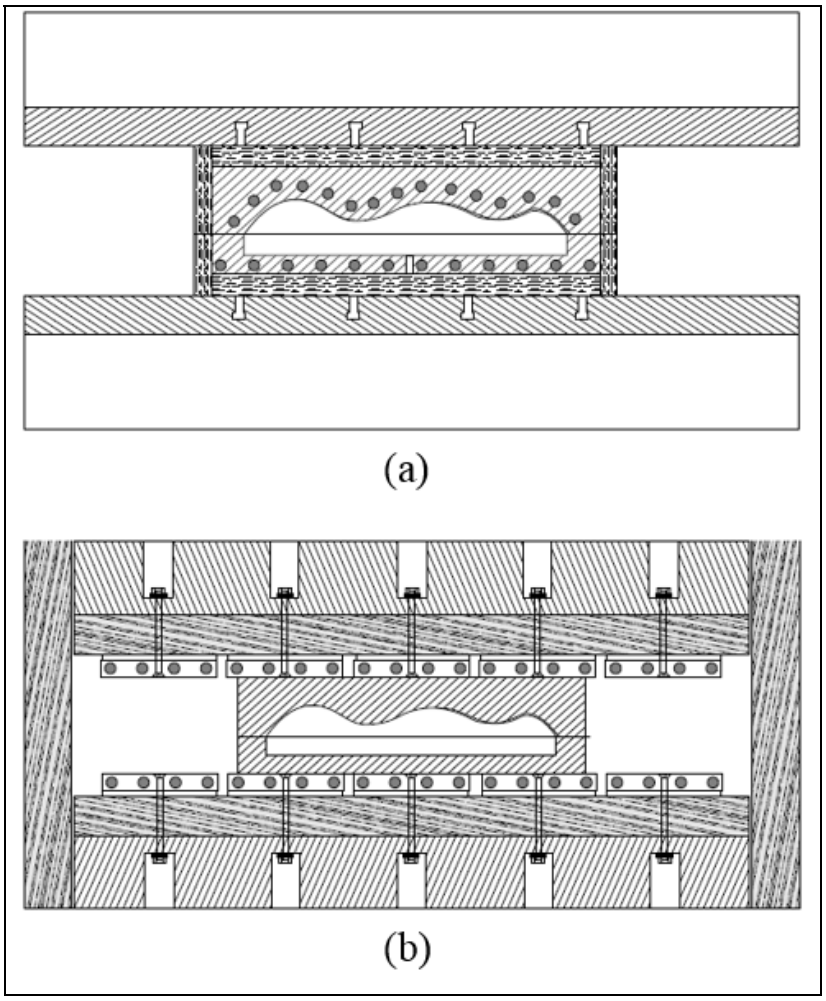

Figure 1-6 Installed heating elements in a SPF/HSBF tool
a) inside the die, b) on the platens
(adapted from (Gillo Giuliano, 2011))

During the offline heating process, the tool is heated in a transient heat transfer mode until reaching the target temperature. Velay et al. (Velay, Cutard, & Guegan, 2008) investigated the thermomechanical loading of a SPF tool during the process for improving the lifetime of the SPF tool. It must be emphasized that in the entire SPF/HSBF process, all types of heat transfer including conduction, convection, and radiation occur under transient conditions.

1.4.1 Conductive heat transfer

During the SPF/HSBF process, particularly in the offline heating mode, the tool experiences the conduction heat transfer in a transient mode when the installed heating elements start heating the tool. Conduction heat transfer occurs in materials where the temperature of two regions is different. When conductive heat transfer varies with time, then the process is called "transient" and in the case of constant heat transfer, it is called "steady state". For an isotropic material without internal heat source the conductive energy equation is expressed as follows (Faghri, Zhang, & Howell, 2010):

$$\rho c \frac{\partial T}{\partial t} = \frac{\partial}{\partial x}\left(k \frac{\partial T}{\partial x} \right) + \frac{\partial}{\partial y}\left(k \frac{\partial T}{\partial y} \right) + \frac{\partial}{\partial z}\left(k \frac{\partial T}{\partial z} \right) \tag{1.2}$$

All terms of the equation are expressed in the nomenclature.

Conduction heat transfer also occurs between the part and the dies, as well as between the insulators and dies. For the numerical simulation of heat conduction, physical properties of the material, ρ, c, and k, are required as mentioned in the above equation. As these terms are variable with temperature, hence, such variations should be considered during the numerical simulation.

1.4.2 Convective heat transfer

Convective heat transfer is the transfer of heat via the motion of fluids. There are two types of convective heat transfer that could be explained as follow:

- Free or natural convection

Natural convection occurs when the motion of a fluid is caused by buoyancy forces. When a fluid is warmed up with a hot source like a hot plate, its molecules are dilated and cause the fluid to be less dense. Consequently, the fluid is dislocated while the cooler fluid becomes denser and the fluid goes down. Thus, the hotter volume transfers heat to the cooler volume of the fluid. The upward flow of air because of a hot object is an example of the free convective heat transfer. Natural convection in SPF/HSBF process occurs between the external surfaces of the tool and ambient air during the offline heating stage. It also occurs during the cooling stage of the process, where there is no cooling media like fans to force the part to be cooled, then, the part is cooled in a free convection mode.

- Forced convection

Forced convection occurs when a fluid is forced to flow over an object by an external source such as fans or sprays. During the cooling stage of the SPF/HSBF process when the part is cooled with a cooling media, like cooling fans, the part is submitted to forced convection. Convection heat transfer is described by the Newton's cooling law, as below (Bejan & Kraus, 2003):

$$\dot{q} = hA(T_s - T_\infty) \tag{1.3}$$

In the numerical simulation of the SPF/HSBF process, the heat convection coefficient (h) is an important parameter that will be discussed in detail through this thesis.

1.4.3 Radiative heat transfer

Thermal radiation is the potential to emit electromagnetic waves from all substances that have a temperature higher than absolute zero. It shows the conversion of thermal energy to electromagnetic energy. Thermal energy is the kinetic energy of movements of molecules in a material. Electromagnetic waves can be propagated in vacuumed spaces. The severity of

emitted energy from a surface depends on the quality and temperature of the surface. When there are two objects with different temperatures, the colder object absorbs the heat by radiation and the hotter object emits the radiation (Howell, Menguc, & Siegel, 2010). In its general form, radiation exchange between two objects is described by the following equation:

$$\dot{q} = \sigma \varepsilon A (T_2^4 - T_1^4) \tag{1.4}$$

In the SPF/HSBF process, radiation phenomenon occurs between the external surfaces of the tool and the ambient atmosphere. However, radiation heat transfer mode is present between all the internal surfaces of the tool. It also occurs, during the cooling stage contributing in the cooling of the part.

In the literature, most of the studies are focused on the material and formability of the SPF/HSBF process part such as (Bruschi, Ghiotti, & Michieletto, 2013; Carrino, Giuliano, & Napolitano, 2003; G Giuliano, Corrado, & Polini, 2018; Lin, 2003; Mikhaylovskaya et al., 2017; Mosleh, Mikhaylovskaya, Kotov, & Kwame, 2019; K Anantha Padmanabhan & Gleiter, 2013; Ridley, Bate, & Zhang, 2005; Yasmeen et al., 2019; Zhao et al., 2017), while, few works are available that consider other aspects of the process like temperature variations and distortion. In the following, some studies related to the thermal aspect of the SPF/HSBF will be reviewed.

1.5 Thermal aspects of the SPF/HSBF process

As mentioned, until now, most of the focus in the studies of the SPF/HSBF process has been dedicated to the material and formability of the process while there are a few works that consider other aspects of the process specifically thermal analysis and distortion. As the temperature variation is one of the most important parameters that affects the final shape of the

SPF/HSBF part, then understanding and analyzing the temperature evolution during the SPF/HSBF process is critical. In the following, a summary of the published literature specifically related to the thermal aspects is presented:

A. Petiot and T. Favre investigated the thermal behaviour of a SPF press and tool to optimize the SPF process with considering tool lifetime, production cycle time, and press productivity. In the study, they simulated the temperature evolution in the press, the SPF tool, and SPF part. In this work, both steady state and transition condition were investigated. The authors concluded that with simulating the heat transfer during the SPF process it will be possible to optimizing the heating cycle, modifying the temperature set-points, and obtaining information in mechanical stresses during the entire process (Petiot & Favre, 2007).

Donato Sorgente et al. investigated the feasibility of conducting SPF process on common industrial presses for the production of an automotive part. In this investigation, they tried to perform SPF of the automotive part with common presses with preparing the required heating power only for the SPF tool. They eventually succeeded to produce the SPF parts with the suggested approach. For the work, they used both experimental and numerical methods but in the numerical simulation they applied different simplifications and presented little information on the boundary conditions they used for their simulations (Sorgente et al., 2016). Fig. 1.7 depicts the SPF part and tool in their study.

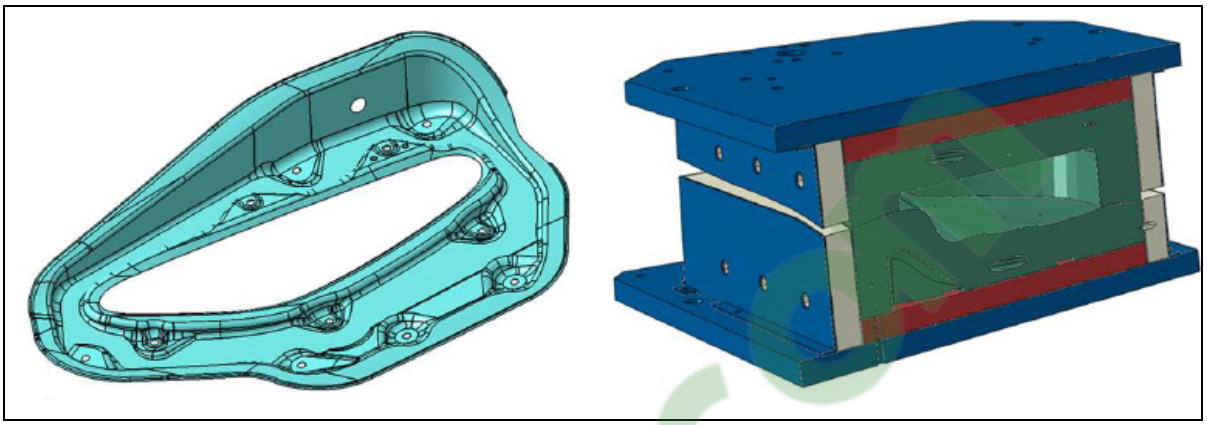

Figure 1-7 The SPF tool and part (Sorgente et al., 2016)

Mauduit et al. examined the feasibility of using infrared lamps for the heating of components during the SPF process. In a laboratory scale, they used several infrared lamps to heat the sheet material for the forming process. In the study, they used both experimental and numerical approaches. They concluded that with using infrared technology the cost of the SPF process would decrease (Mauduit, Le Fournier, Grondin, Pottier, & Le-Maoult, 2017). Fig. 1.8 illustrates the schematic section view of the used approach in this investigation.

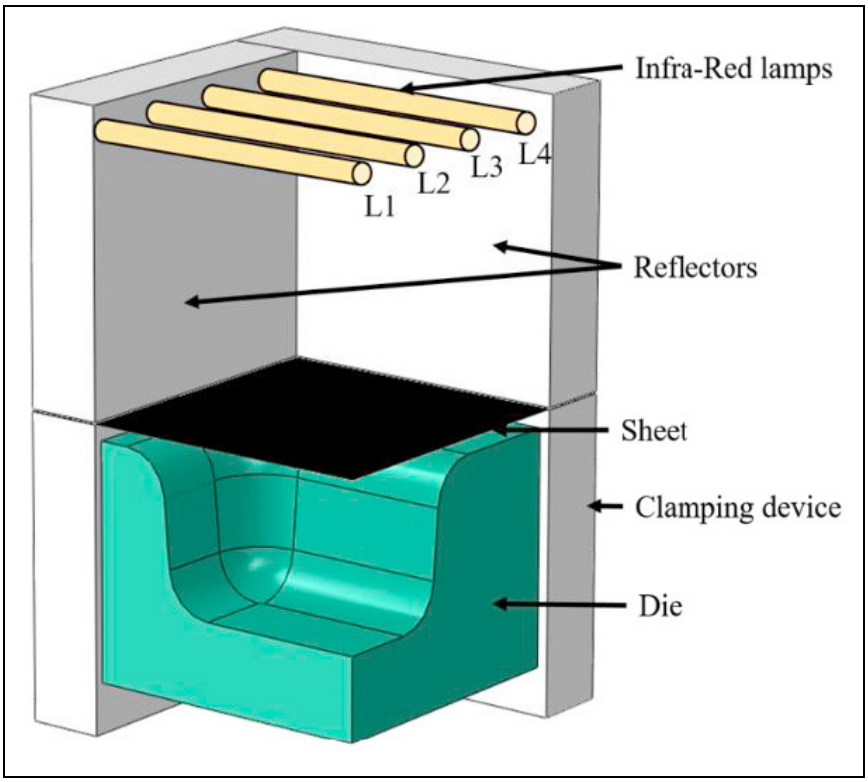

Figure 1-8 The schematic section view of the applied laboratory scale aparatus (Mauduit et al., 2017)

1.6 Distortion phenomenon during the SPF/HSBF process

Generally, distortion in a solid component occurs when the component is exposed to disparate (non-uniform) contraction or expansion. This phenomenon usually occurs when a part is in a manufacturing or heat-treating process. Fig. 1.9 shows a sample of a distorted part after a quenching process.

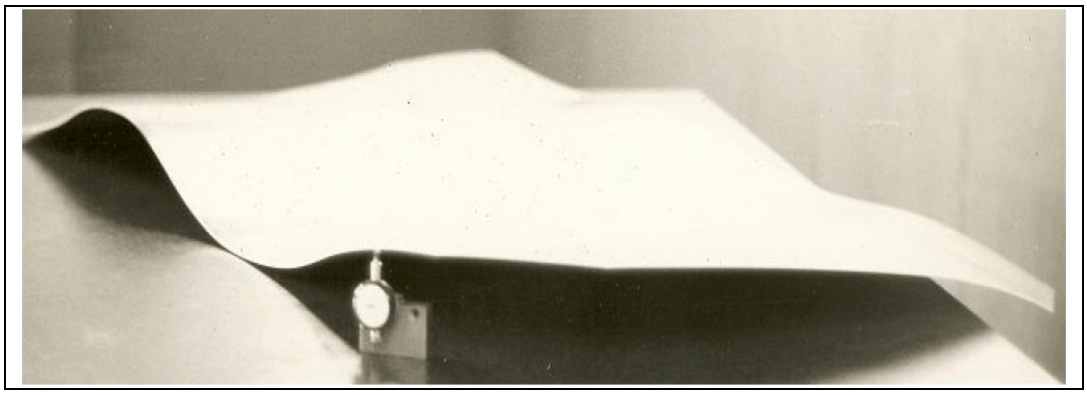

Figure 1-9 A distorted part after quenching process (CROUCHER, 2008)

Distortion in a part is a complex phenomenon which depends on different parameters like geometry, metallurgical structure, temperature variation, residual stresses, mechanical boundary conditions, etc. (Chandler, 1996; CROUCHER, 2008; Totten, 2002). Distortion could occur in different industrial processes such as welding, quenching, and machining. In this regard, many efforts have been made to predict and control this phenomenon. Practically when a part distorts, its desirable shape and dimensions will be affected, then rework is required which is an adding cost to the part. Fig. 1.10 illustrates the influence of different effective parameters on the distortion in a part. One of the conventional industrial processes on the metallic materials is cooling. The cooling process is usually applied after heat treating or hot deformation processes. As the SPF/HSBF process is carried out at high temperature then a cooling step is always used to cool down the part after the deformation process.

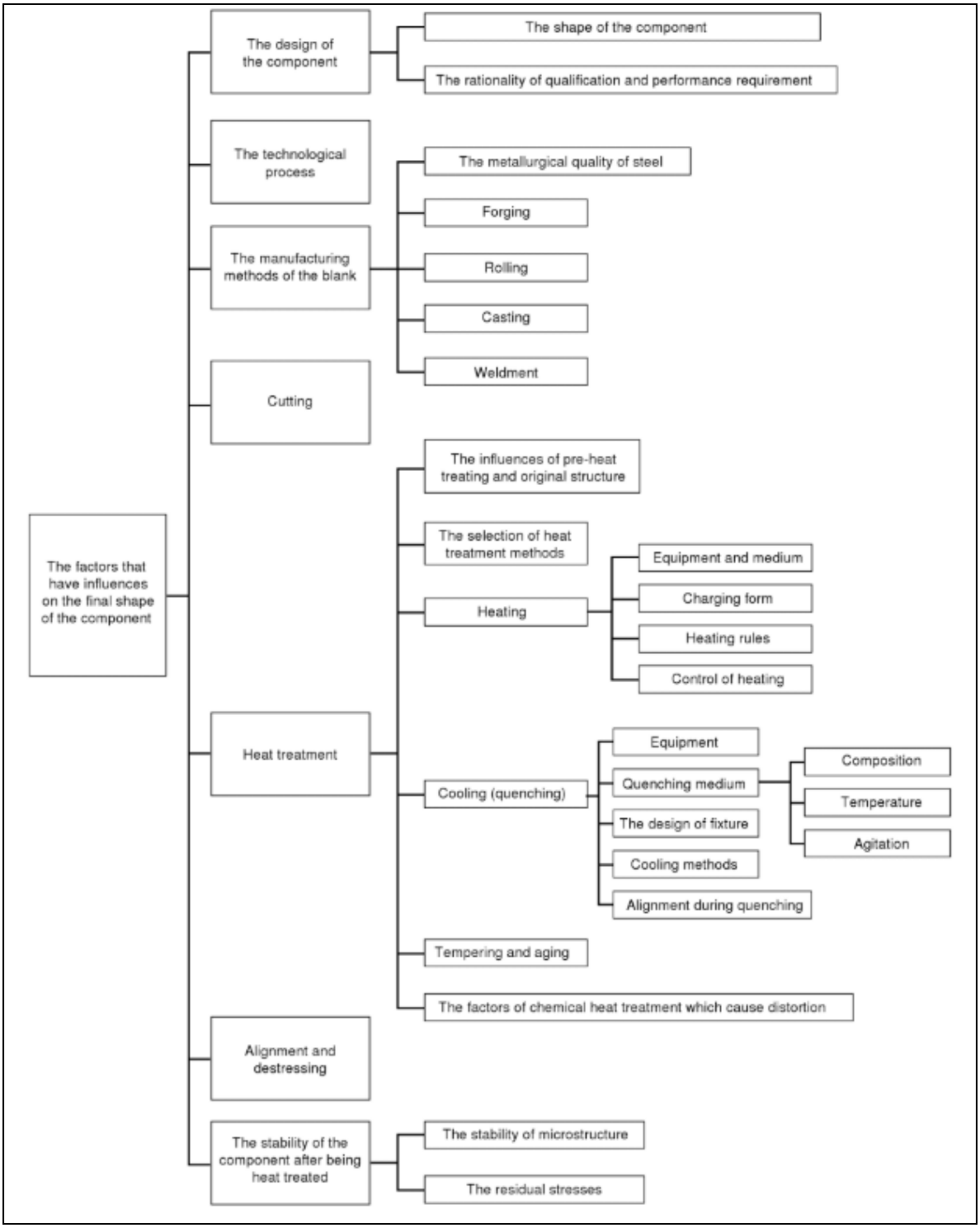

Figure 1-10 Effective factors on the distortion phenomenon (Totten, 2002)

1.6.1 Thermal analysis of the SPF/HSBF process

For the thermal analysis of the SPF/HSBF process, both experimental and numerical approaches could be employed. In the thermal analysis, recording temperature evolution during the process is required which is usually performed by attaching thermocouples (TCs) at different locations of the die or the sheet material. This approach is also applied in this study. Fig. 1.11 shows an example of attached thermocouples on a sheet material and die of a hot stamping process.

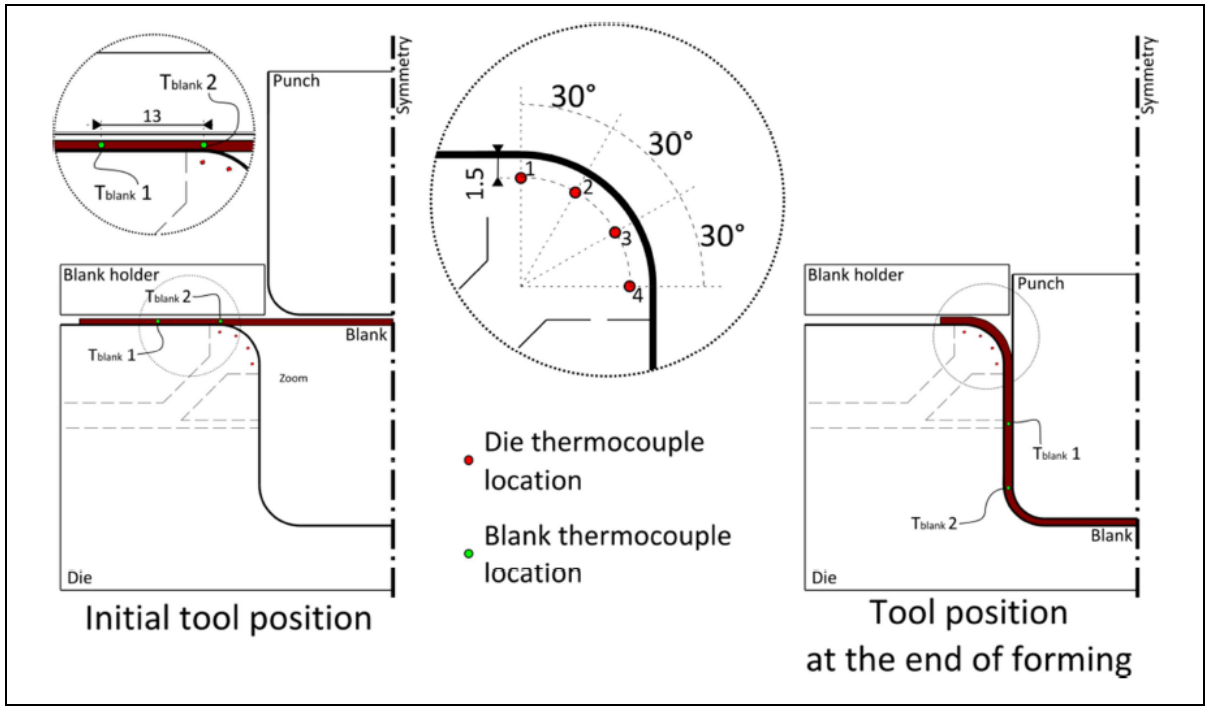

Figure 1-11 Attached thermocouples at the different locations of a sheet material and die in a hot stamping process (Blaise, Bourouga, Abdulhay, & Dessain, 2013)

For the numerical modelling of the temperature evolution during the SPF/HSBF process, the accurate determination of the thermal boundary condition is essential. As mentioned above, during the SPF/HSBF process, all modes of heat transfer occur and beside the boundary

conditions, the right physical properties of the materials (material of the sheet and tool) should be considered.

In the numerical modelling of the part during the cooling process, one of the most important parameters is Heat Transfer Coefficient (HTC) that should be determined. For the calculation of the HTC value during the cooling processes, usually temperature evolution curves are used (Liščić, 2016; Zhang, Feng, Li, & Liu, 2013), which is similarly employed in this thesis. In this method, the condition of the conductive heat transfer within the part is determinative. If the internal conduction within the part is negligible then the HTC value could be directly calculated from the cooling curves but in the case when the internal conduction is significant then the calculation of the HTC is challenging and usually inverse method (Huiping, Guoqun, Shanting, & Yiguo, 2006; Xu, 2006) is applied for the calculation purpose.

The criterion for the determination of the HTC value by inverse or direct method is the Biot number. The Biot number is defined by:

$$Bi = \frac{hl}{k} \tag{1.5}$$

If Bi is less than 0.1, then the internal conduction could be ignored (Bergman, Incropera, Lavine, & DeWitt, 2011). In this thesis, due to the very low thickness of the blank (about 2 mm), internal conduction within the SPF part could be ignored and the HTC value for the part is determined directly from the cooling curves by considering the energy balance equation for the workpiece. Xiao et al. employed this method in for calculating the HTC value for a work piece (Xiao et al., 2011). The authors used the following relation (equation 1.6) for the calculation of 'h' and Fig. 1.12 shows the evolution of HTC with temperature using the above method:

$$h = \frac{mc}{A(T_{part} - T_{air})} \cdot \frac{dT}{dt} \tag{1.6}$$

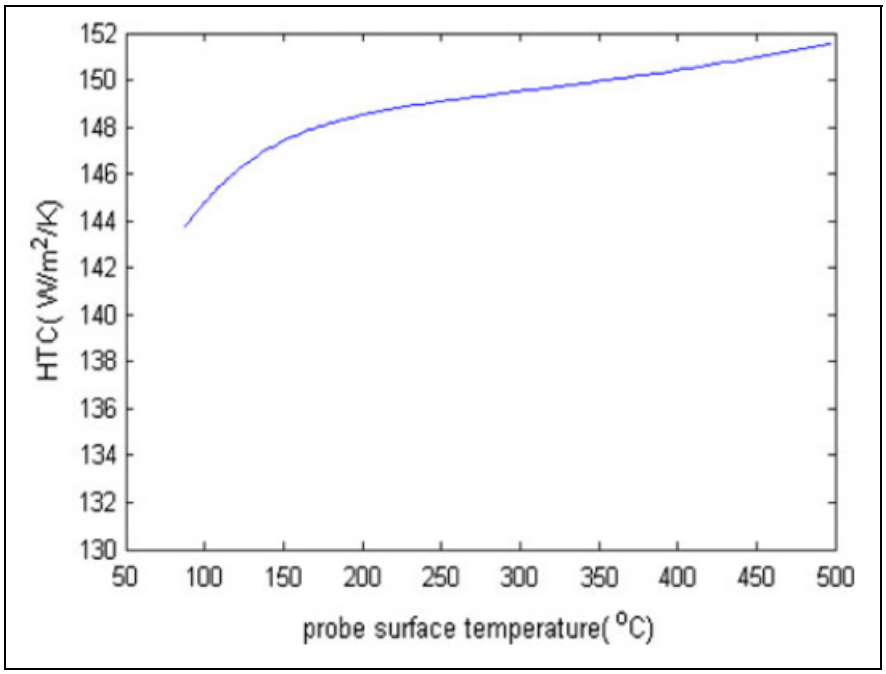

Figure 1-12 Calculated HTC value vs workpiece temperature (Xiao et al., 2011)

During the cooling processes, usually the cooling media is a liquid such as oil or water, which makes the cooling process quite fast that is named quenching. The HTC values in the quenching processes are significantly higher than that of air/gas cooling processes. In the air/gas cooling processes the range of the HTC value is about several hundreds while in the quenching it shows several thousands. It should be noted that in the air/gas cooling cases, if the air/gas is applied under pressure or high speeds, then the HTC values could be comparable with the quenching processes in the liquid media. Fig. 1.13 depicts a graph of HTC value in a liquid media with values reaching above 5000 during the quenching process.

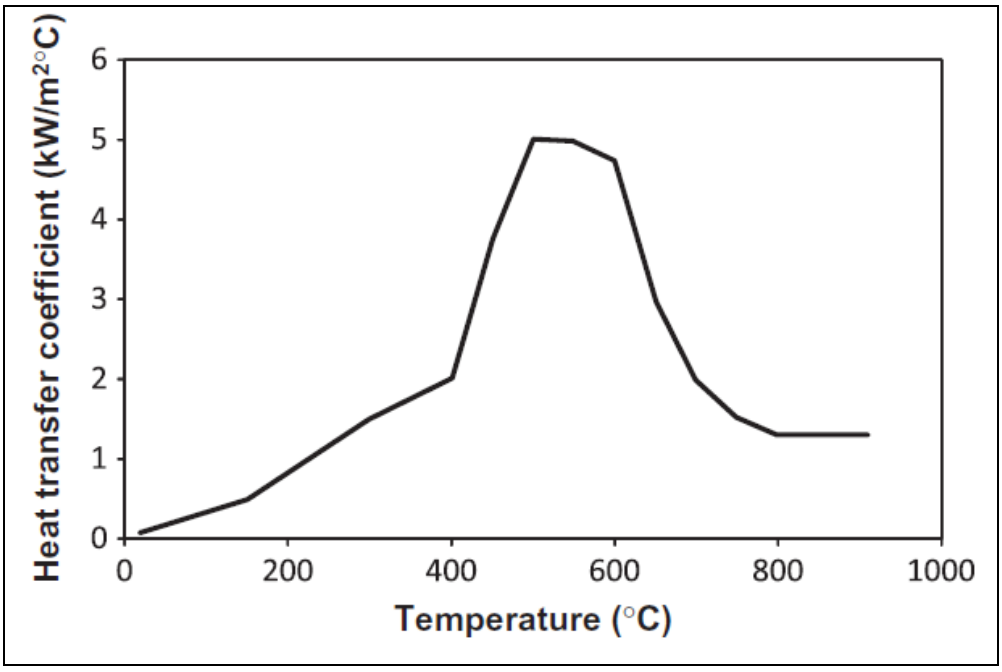

Figure 1-13 HTC value for a steel component quenched in an oil media (Da Silva et al., 2012)

However, in most cases of the SPF/HSBF process the cooling step is performed in the ambient air with/without air blowing to the part, hence the range of the HTCs would not be more than few hundreds. Therefore, in this work the effect of the radiation term in the total heat transfer was investigated.

It must be also noted that fluctuations have been observed in the values of the calculated HTC when using the above mentioned method (Kim & Oh, 2001). Fig. 1.14 shows an illustrative example of the HTC fluctuation during an air cooling process. The observed fluctuations have been related to temperature recording and considered as measurement background noise.

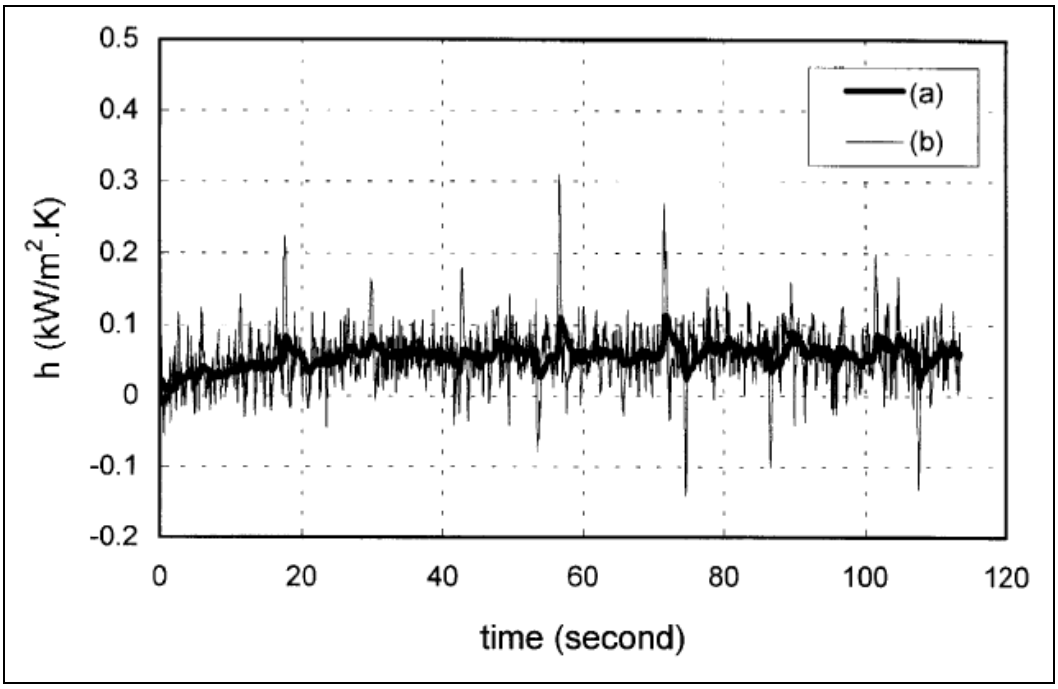

Figure 1-14 HTC value with fluctuation in air cooling process (Kim & Oh, 2001)

However, Xiao et al. (Xiao et al., 2011) reported that this background noise could lead to significant error in the calculation of the cooling rate and the HTC value. Hence, to avoid such error, they used a smoothed cooling curve profile by employing a polynomial function and then the smoothed data was used to calculate the HTC and cooling rate. In their calculation, no details were provided on the possible induced error in the calculation of the HTC or cooling rate. Fig. 1.15 depicts a comparison of the cooling curves in the original and smoothed data in their study.

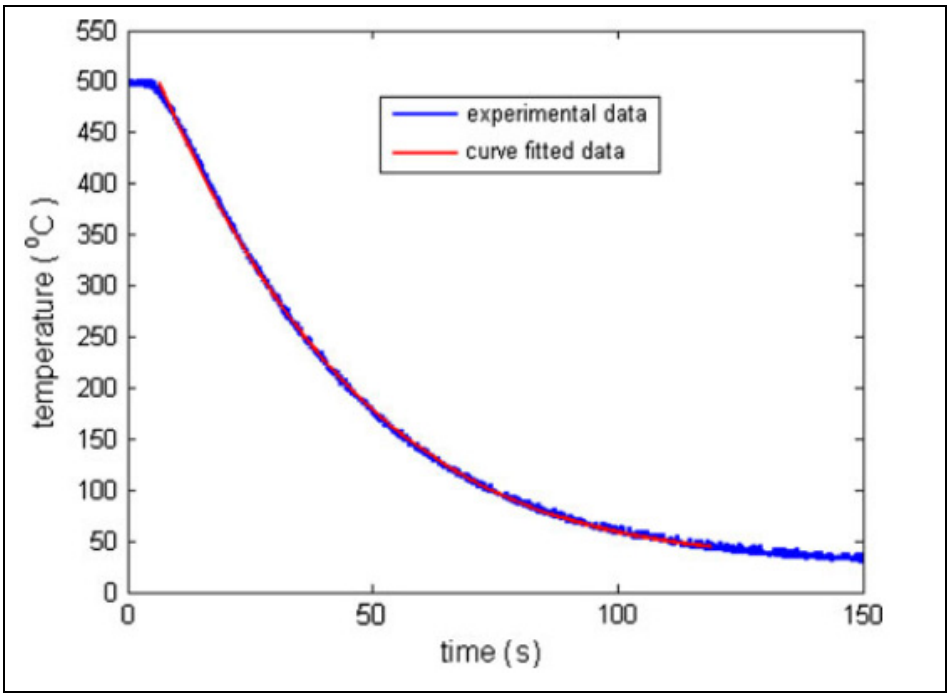

Figure 1-15 Comparison of the cooling curves data in original and curve fitted states during air cooling process (Xiao et al., 2011)

In this thesis, for the calculation of the HTC, both original cooling curve data and curve fitted ones were used and the numerical results based on both approaches were compared.

1.6.2 Studies on the distortion phenomenon

As mentioned above, little information is available on the cooling process of SPF/HSBF components including thermal analysis and distortion issues. Moreover, among the few available studies, very little or no detailed information is provided on the above topics.

Generally, distortion in a component means deviating from the original shape and dimensions. This could occur in any component with different dimensions. However, distortion due to the cooling process could occur in different media with different conditions such as still air, blowing air, still oil, agitating oil, etc. Due to the different conditions of the cooling processes, distortion is considered as a complex phenomenon in a vast range of applications (Deng & Murakawa, 2008; Hou et al., 2012; Li et al., 2020; Prantil, Callabresi, Lathrop, Ramaswamy,

& Lusk, 2003; Priesnitz, Sinke, & Benedictus, 2014; Sonar, Lomte, Gogte, & Balasubramanian, 2018).

For example O. Kessler et al. (Kessler et al., 2006) investigated and compared the effect of high pressure gas quenching and liquid quenching on the distortion of an aluminum alloy sheet part. In their study, they found that high pressure gas quenching could reduce the distortion in the part in comparison with the liquid quenching process.

Yang et al. (Yang et al., 2013) simulated the quenching process of a thin large part made of aluminum alloy using the finite element software ABAQUS. In their analysis, they used three types of quenchant and compared the quenching results of each experiment. They emphasized that for the modelling of the process accurate determination of the HTC value is critical. In their work, they did not discuss how they measured the distortion reported in the paper. Fig. 1.16 shows the part that they used for their work.

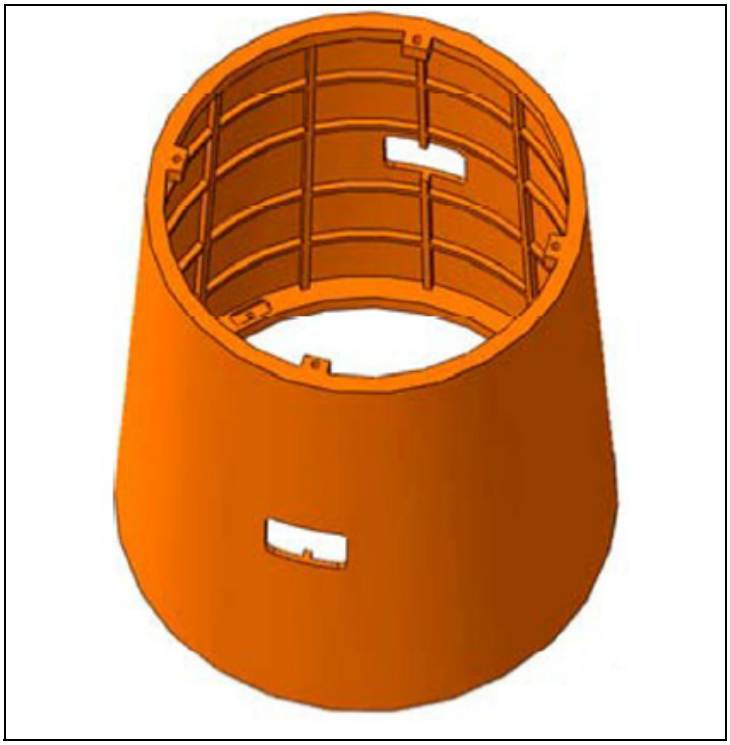

Figure 1-16 The large thin aluminum alloy part used in Yang et al work (Yang et al., 2013)

Rollin et al. (Rollin et al., 2016) simulated the forming, cooling, and clipping process of a SPF part with ABAQUS. In the numerical modelling of the cooling process, they applied three different strategies to investigate the effect of the temperature distribution and evolution on the distortion phenomenon. They stated that these strategies were not consistent with the real working conditions. Consequently, there was no validation of the numerical results.

Bikass et al. (S. Bikass, B. Andersson, A. Pilipenko, & H. Langtangen, 2012) worked on a simple extruded aluminum plate to investigate the effects of non-uniform cooling process on the distortion phenomenon. Fig. 1.17 shows the part and different non-uniformities cases. Generally, they concluded that, increasing in the non-uniformity would result into more distortion of the part. Their work clearly shows the effect of the thickness non-uniformity on the distortion. Non-uniformity in the thickness of a SPF/HSBF part is normal according to the nature of the process. Hence, it could be noted as one of the effective factors on the distortion of the part.

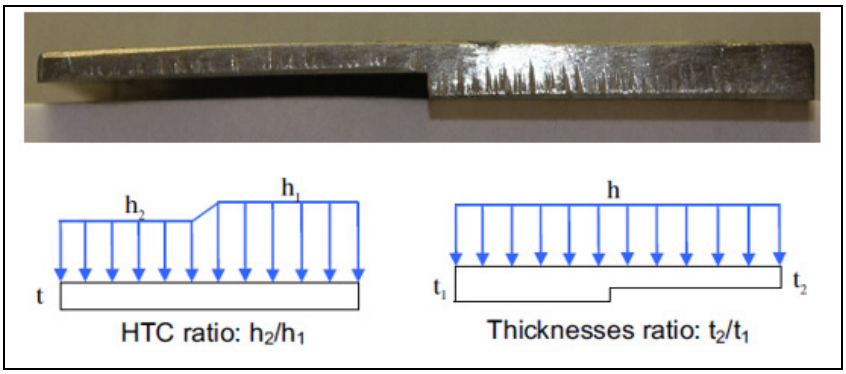

Figure 1-17 Extruded sample and schematic of non-uniform cooling (S Bikass et al., 2012)

Xiao et al. (Xiao et al., 2011) conducted several experiments to study the influence of forced air cooling on distortion of a cast aluminum part. The authors examined the effects of the air temperature, humidity, and velocity on the workpiece from different directions. Fig. 1.18 illustrates the schematic of the workpieces in different directions used in the experiments. As one of the concerns of the work was the distortion of the part after the cooling process, they specially focused on the determination of the HTC to find the best cooling strategy for optimizing the process. They calculated the HTC directly from the cooling curve of the workpiece, a method that was also adopted in this thesis. They concluded that the HTC value was significantly dependent on the air velocity and workpiece orientation but much less sensitive to the air temperature or humidity.

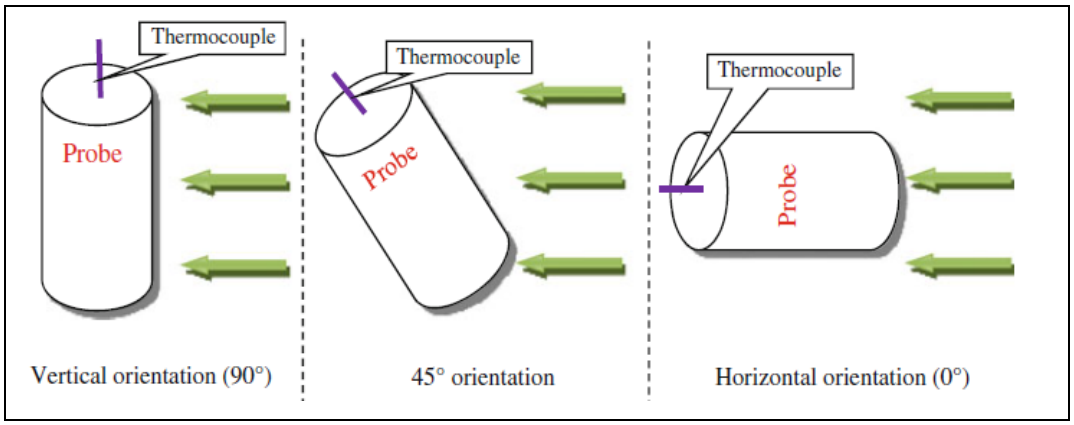

Figure 1-18 The schematic workpieces with different directions (Xiao et al., 2011)

1.7 Conclusions (challenges and objectives)

The above literature review shows that the thermal aspects of the SPF/HSBF process have not been developed specifically when it comes to the thermal analysis and distortion issue in the SPF/HSBF components. Although SPF itself has been utilized for more than forty years but most of the attentions in this method was paid to the material and formability. Beside this concern, SPF is inherently suffering from the high cycle production time because of the low strain rate used for the forming process. Hence, HSBF was recently introduced as an alternative technique with a production cycle time sometimes 20 times faster than that of SPF. However, both SPF and HSBF are expensive techniques and attention must be paid to reduce rework or scrapping at the end of the process.

It must be emphasized that SPF/HSBF is a complex thermomechanical process and the tool and part during the process are exposed to significant temperature variations. The components experience high temperature gas/air blowing during the forming process and then cooling usually with still or blowing air. As a result, distortion as a common issue occurs in the final step of the process which is subject to rework or rejection. Therefore, investigating the problems due to the temperature variation during the entire process is of crucial importance and this thesis is aimed to develop thermal analysis in the SPF/HSBF process.

For running the production line of a SPF/HSBF process, the SPF/HSBF tool is required to be heated until a target temperature close to 500ºC in the forming of an aluminum alloy case. The heating process is usually performed out of the press through offline heating. According to the significant volume and mass of the tool, this process could take up to 30 hours in the present study, which is a quite long process. For optimizing purposes, shortening this long heating period could be a valuable investigation which has not been considered in the literature.

For the heating of the tool, usually heating elements, as the source of heat supply, are utilized. Depending on the design, the heating elements are installed in different locations of the SPF/HSBF tool and a controlling system such as PID drives the heating process. The offline heating process begins from the ambient temperature to the target temperature which is a transient heat transfer state. After reaching the target, temperature will change in a limited range during the production process, which is like a semi steady state. At the end of the offline heating process, temperature distribution on the surface of the dies (upper and lower) is critical since it is transferred on the part at the end of the forming process. In other words, the temperature distribution on the part at the beginning of the cooling step follows the temperature distribution of the die at the end of the forming process. As the temperature distribution on the part is critical in the cooling process then the temperature distribution on the part should be well considered. In general, more uniformity in the temperature distribution on the die is desirable, hence, one of the important goals in the thermal management of the SPF/HSBF tool should be the uniformity in the temperature distribution of the dies. In the literature, such consideration have not been taken into account and there is little available information with not much details, while temperature variations in the different steps of the SPF/HSBF process affects other steps and the thermal analysis is an interconnected process.

Usually in the cooling/quenching processes, the initial temperature distribution of the cooled/quenched part is uniform and it is not considered as a source of any problem in the literature. This is mostly because of the nature of the heat-treating process in which the part is

heated for several hours and presents a uniform temperature distribution even in the large and thick parts. Sometimes, this uniformity is presented due to the smallness of the part. However, in the real process, the temperature distribution on the surface of the SPF/HSBF die is not uniform. On the other hand, the SPF/HSBF parts are thin and usually large, then the initial temperature distribution at the beginning of the cooling process is not uniform. This fact in the process, makes the thermal analysis of the cooling process more challenging specifically when it comes to calculating the HTC value. Practically the instantaneous HTC value will not be uniform within the part during the cooling process which makes the calculation more complex.

Another lack of practical knowledge in the SPF/HSBF is the measurement of the distortion. In most cases, authors do not point how they practically measured the distortion in the real parts. In this thesis, the detailed distortion measurement methodology is considered.

Based on the above investigation this thesis has been defined to achieve the following objectives as detailed below:

1) Performing a comprehensive and thorough thermal analysis and obtaining a reliable numerical model that can correctly predict the temperature evolution in the tool during the entire process of the offline heating. In the practical case of this thesis, since the heating sources of the SPF/HSBF tool are governed by PID controllers, then a good knowledge of the PID controllers is required to be able to correctly apply the thermal boundary conditions. As all modes of heat transfer occur during the process and the tool is made of a different material, then, all the material and process parameters should be well determined. The obtained model should be validated with experiment(s) and based on the validated model, an optimized offline heating process will be determined with the view to minimize the duration of the offline heating process and maximize the uniformity in temperature distribution of the surface of the dies at the end of the process.

2) Experimentally and numerically studying and analyzing the temperature evolution in the SPF/HSBF part during the entire cooling process. In this section, recording the

temperature evolution of the part during the cooling process is required. Based on the temperature recording, the HTC value should be determined which is the most important parameter in the numerical simulation. The most challenging part of this section is the calculation of the HTC value. The actual SPF part is large and the initial temperature distribution is not in reality uniform. On the other hand, the applied blowing air (from cooling fans) on the part does not actually present a uniform flow on the surface of the part, then each point over the part will have a different HTC value. Therefore, there should be a reasonable solution to overcome the challenge. The solution will be presented in the coming chapters.

3) Experimentally investigating the distortion issue by conducting different experiments and proposing mitigation measures to reduce/overcome the issue. In this portion of the work, different experiments will be designed and conducted to investigate the effect of various parameters on the distortion of the SPF part. One of the challenges in this section will be the measurement of the distortion through the parts. As the experimented parts are large and the final shape of them are going to be compared with the original part, then the measurements should be accurate enough. In this regard, for a reliable and qualified measurement, use of a 3D scanner camera will be considered. These cameras use point cloud methodology having a high precision and accuracy.

CHAPTER 2

FINITE ELEMENT AND EXPEIMENTAL ANALYSIS OF THE PREHEATING STAGE OF HIGH SPEED BLOW FORMING (HSBF) PROCESS

Alireza Aleyari[a] , Omid Majidi[a], Nicolas Bombardier[b],Xuan-Tan Pham[a], Mohammad Jahazi[a]

[a] Department of Mechanical Engineering, École de Technologie Supérieure (ETS), Montreal, QC, H3C 1K3, Canada

[b] Verbom Inc., 3820 boulevard Industriel, Sherbrooke, QC, J1L 2V1, Canada

Paper published in the journal of *Manufacturing Processes,* In November 2019

Abstract

High-Speed Blow Forming (HSBF) is a new manufacturing technology based on superplastic forming for the production of complex shape thin sheet of aluminum alloys for electrical car body panels. A major challenge for the full scale industrialization of the process in automotive industry is to reduce the overall HSBF processing time while keeping temperature distribution as uniform as possible on the dies. In this study, the thermal mapping of the dies during the preheating cycle (also known as offline heating) of a HSBF process was investigated using a hybrid experimental-numerical method with a view to minimizing the preheating time and to obtain a uniform temperature distribution on the dies surfaces at the end of the preheating cycle. To this end, the upper and lower dies of an industrial size part were instrumented with 14 thermocouples at different locations of the dies. The process was simulated using the finite element software ABAQUS to predict the temperature evolution over the entire surfaces of the

dies from room temperature to the target temperature. The predictions were validated by comparison with the experimental measurements. Based on the obtained results a new offline heating cycle insuring minimum discrepancy in temperature distribution and minimum processing time is proposed.

Keywords: Superplastic Forming Tool, Heating Element, Offline Heating, ABAQUS.

2.1 Introduction

High-Speed Blow Forming (HSBF) is a newly introduced manufacturing process in which a superplastic sheet metal is deformed to very large strain levels (200 % to 1000 %) in order to shape complex geometries that could not be obtained using traditional metal stamping methods. The most contrasting feature of the HSBF process is the higher strain rate when compared to a conventional Super Plastic Forming (SPF) process. HSBF process is usually carried out at high temperatures between 0.4 to 0.6 of melting point of the sheet material (T_m), and strain rates of around 10^{-2} s^{-1}. Due to the complexity of the shape of the formed parts, thinning, rupture, wrinkling, distortion, and galling could occur at different stages during or after the process. It has been reported that local variations of temperature, strain rate, friction coefficient, and the microstructure of the material have significant impacts on the quality of the SPF products (Cappetti, Garofalo, Naddeo, Nastasia, & Pellegrino, 2010; Gillo Giuliano, 2011). Therefore, in order to increase reliability and repeatability of the HSBF process, it is crucial to develop a better understanding of each step of the process. However, due to the recent introduction of this technology, little data is available in the literature and most of the existing reports are focused on the mechanical properties and formability of the material rather than thermal aspect of the process. The data is even scarcer on complex shape thin sheet of aluminum alloys formed by the HSBF technique.

Fig. 2.1 shows schematically the main steps of the HSBF process which include preheating of the forming dies outside the press (known as offline heating), preheating blank in the hot die, preforming the blank by crash forming, gas blowing, and the final cooling process. Among the

above variables, temperature has one of the most significant impacts on the quality of the final product. Often a combination of experimentation and numerical simulation, mostly finite element analysis (FEA), has been used to quantify and analyze the influence of temperature on the forming process.

For example, Velay et al. (Velay, Cutard, & Guegan, 2012) investigated the influence of thermal loading cycle on thermomechanical stresses and strains induced on a superplastic forming die using FEA. Mis et al. (Mis, Hall, Spence, Emekwuru, & Kibble, 2013) used FEA to study the impact of temperature distribution and heat transfer management on the quality of the final product in a SPF process. Harrison et al. (Harrison, Rubek, & Friechnan, 2013) developed a FEA based method to optimally design and determine the heat sources and insulators in a hot stamping die to achieve desired temperature distribution in the die. Recently Mauduit et al. (Mauduit et al., 2017) reported that it is possible to use infra-red lamps to directly heat up the sheet material during superplastic forming process. Xiao-bo et al. (Fan, He, & Yuan, 2012) studied the forming behavior of 5A06 aluminum alloy sheet during hot gas forming process and highlighted the importance of temperature, pressure and time on the formability of the aluminum sheets during the process. Sorgente et al. (Sorgente et al., 2016) investigated the feasibility of using a common industrial press with a different heating approach to form components with SPF process.

Due to the large mass of the HSBF tool (in general more than four metric tons) heating it to the target temperature (~500 ºC) takes often more than 30 hours. Thus, from a production optimization point of view, the dies are usually heated to near the target forming temperature outside of the press (offline heating). Then a small portion of the heating process is carried out after mounting the tool on the press (online heating). However, from a quality perspective, it is crucial that the heating process does not result in unacceptable temperature distribution within the die, particularly considering the complex geometry of the part. Therefore, an in-depth understanding of the interactions between material properties, die geometry, and heat

transfer needs to be developed to insure reliability and repeatability of the manufacturing process. A better understanding of temperature history during the offline heating will also contribute to the development of an optimized heating strategy thereby improving production rate and reducing energy consumption.

The present study has been defined in this context and its main objective is to investigate the temperature evolution during the *offline* heating step of the HSBF process of thin sheet of aluminum alloys for automotive applications. To this end, an industrial size HSBF tool, used for a large size complex shape part, was fully instrumented with thermocouples and temperature evolutions were recorded during the offline heating process. A numerical model using ABAQUS was developed to simulate the different stages of the heating process and predict the temperature evolution over the surfaces of the upper and lower dies. Special attention was paid to the selection of heat transfer coefficient, material properties, and other boundary conditions considering the actual industrial conditions. Finally, the numerical predictions were validated with the experimental results that helped defining new heating strategies for better uniformity and shorter heating times. In the next sections, the applied experimental and FEA procedures will be described and the results will be discussed.

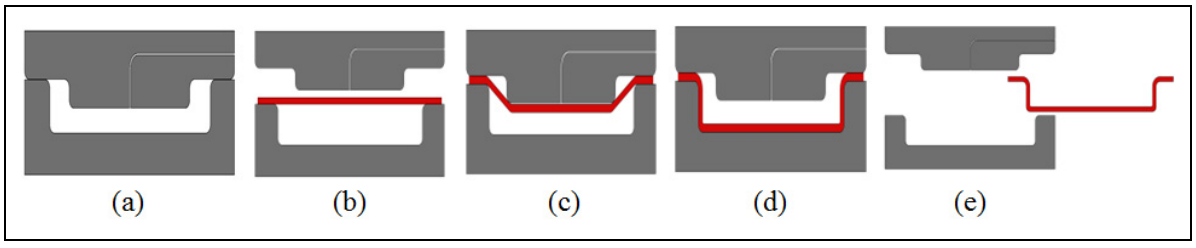

Figure 2-1 The schematic of a HSBF process a) offline heating of the tool, b) heating of the sheet material, c) preforming, d) blow forming, e) cooling

2.2 Experimental procedures

The HSBF tool consists of two heating platens and two dies (i.e. lower and upper). The heating platens have approximate dimensions of 1.5 m×1.5 m×0.5 m and are used for different dies. Fig. 2.2 shows the cross section view of the CAD model of the studied HSBF tool. In order to

provide the required energy for heating the tools, thirty flexible tubular heating elements of 3735 W were installed on the surface of the heating platens. The heating elements are controlled using a PID (Proportional-Integral-Derivative) controller during the entire process. In order to monitor and control the temperature of the dies, 14 type K thermocouples (TC) were fixed 2 mm below the surface of the dies through drilled blind holes from the back of the dies. As also shown in Fig. 2.2, during the heating process, the upper and lower heating platens are completely closed. Fig. 2.3 shows the locations of the TCs that were chosen carefully to cover the entire area of the lower and upper dies. Based on preliminary experiments, TC8 was selected as the controller thermocouple for the operation of the PID and temperature of all TCs were recorded every second using a conventional data logger. The preliminary experiments helped having an initial estimation of temperature distribution on the surface of the die to determine how sophisticated the controlling system should drive the heat sources to obtain an optimal temperature distribution on the surface of the die. As the experiments did not show considerable discrepancy in the temperature distribution (less than 25 ºC) therefore the analysis was focused on using one controlling temperature. For the analysis TC8 was selected; however, any other TC could have also been used. Furthermore, to minimize thermal shocks a heating rate below 60 ºC/hour and limited power were initially applied.

On the basis of the above criteria, during the first step of the heating process, a constant power was provided to the elements for almost 13 hours. The voltage was then increased to 600 V until the target temperature was reached with a heating rate determined by the PID system.

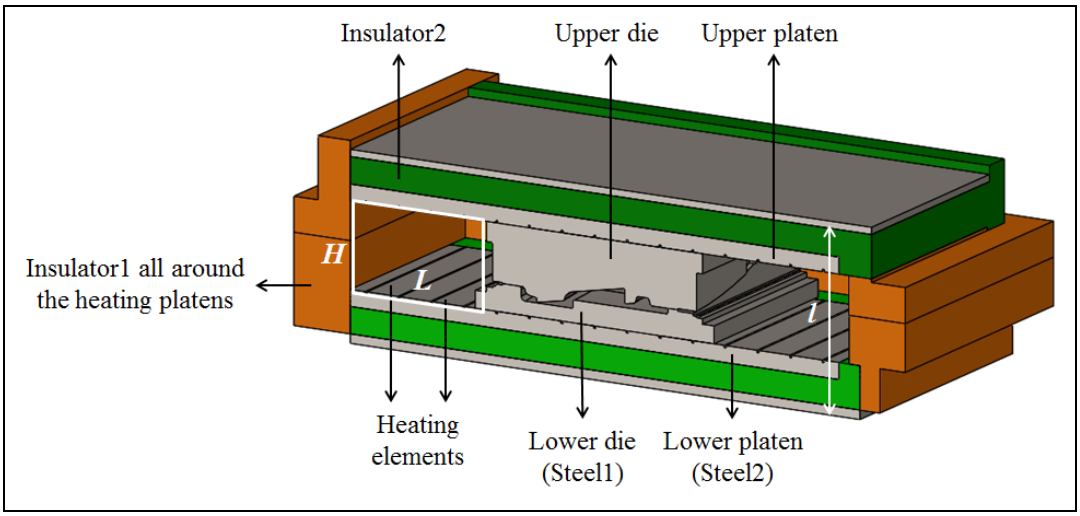

Figure 2-2 The CAD model of the HSBF tool

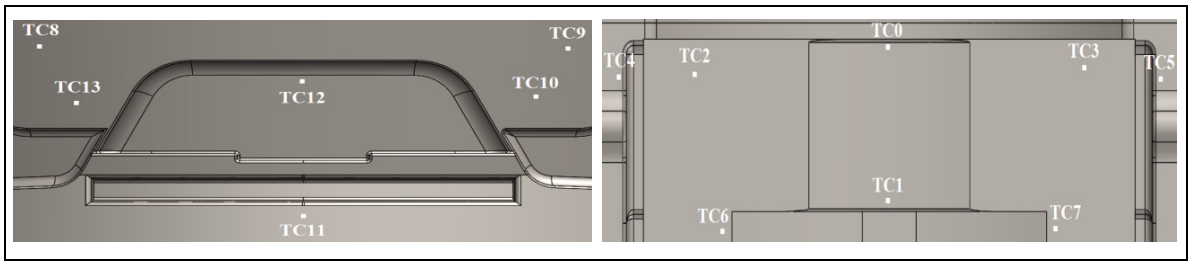

Figure 2-3 Positions of the TCs on the upper and lower dies

2.3 Numerical model and boundary conditions

ABAQUS 6.13 was used for the numerical simulations and the CAD files were prepared by CATIA V5R21. A total number of 429477 linear tetrahedron elements (DC3D4) were used for meshing of the assembly.

The HSBF dies, plates and insulators are made of different materials with different physical properties, as reported in Table 2.1. The die material is made of steel 1, and the upper and lower plates from steel 2. The insulators were placed between the heating platens and the outer surface.

Table 2-1 Material physical specifications

	Density (Kg/m^3)	Specific heat capacity (J/kg ºC)	Conductivity (W/m ºC)
Steel1 ("https://www.verbom.com (supplier of the HSBF die),")	7860	460	34
Steel2 ("https://www.verbom.com (supplier of the HSBF die),")	7850	490	43
Insulator1 ("http://www.bnzmaterials.com (material producer),")	961	1260	0.17
Insulator2 ("http://www.industries3r.com (material producer) ")	138	1050	0.11

The above physical properties for the steels vary with the temperature. In the range of this study (20 ºC – 500 ºC) according to the low impact of the variable properties they were considered as constant. Furthermore, the temperature of the insulators did not increase considerably hence similarly their physical properties were also assumed as constant. According to the well machined and smooth surfaces the contacts between the all surfaces were considered almost ideal.

During the offline heating process, the HSBF tool stands on four legs and natural convection heat transfer was assumed to occur both internally and externally. Moreover, radiative heat transfer was assumed between all internal surfaces and externally between the surfaces and the ambient atmosphere. For all surfaces, an emissivity ($\boldsymbol{\varepsilon}$) value of 0.8, corresponding to a mild oxidized steel surface (Wilson, 2004), was considered. The ambient temperature and the initial temperature of the HSBF tool were considered equal to 20 ºC.

For the calculation of the external heat convection coefficient, *h*, the surfaces were considered as flat plates and the following relations reported in (Çengel & Ghajar, 2011) were used:

$$h = \frac{Nu.k}{l} \tag{2.1}$$

$$Nu = C.Ra^{n} \tag{2.2}$$

$$Ra = \frac{g\beta(T_s - T_\infty)l^3}{\nu^2}.Pr \tag{2.3}$$

where Nu is the Nusselt number, k the air thermal conductivity (W/m ºC), l the characteristic length (m) , Ra the Rayleigh number, Pr the Prandtl number, T_s the surface temperature (ºC), T_∞ the ambient temperature (ºC), g the gravity (m/s²), β the air thermal expansion coefficient (1/K), ν the air kinematic viscosity (m²/s), and C and n are constants.

It should be noted that, in the above equations a constant surface temperature (T_s=*constant*) is assumed; however, in practice, the temperature of the surfaces are not exactly constant and some variations occur. Therefore, the average of the initial and end temperatures that was experimentally measured was considered as T_s. Finally, the other constants (*k*, *v*, etc.) were obtained from [13].

Table 2.2 summarizes the *h* values used in each step and related constants for the upper, lower, and side plates.

Table 2-2 External heat convection coefficients and related parameters

	Upper surface	Lower surface	Lateral surfaces
First step	$T_s = 25$ $\beta = 0.0034$ $k = 25.3\times10^{-3}$ $\upsilon = 1.54\times10^{-5}$ $Pr = 0.73$ $C = 0.15$ $n = 1/3$ $l = 0.47$ $h = 3$	$T_s = 25$ $\beta = 0.0034$ $k = 25.3\times10^{-3}$ $\upsilon = 1.54\times10^{-5}$ $Pr = 0.73$ $C = 0.27$ $n = 1/4$ $l = 0.47$ $h = 1.2$	$T_s = 25$ $\beta = 0.0034$ $k = 25.3\times10^{-3}$ $\upsilon = 1.54\times10^{-5}$ $Pr = 0.73$ $C = 0.59$ $n = 1/4$ $l = 0.68$ $h = 2.5$
Second step	$T_s = 80$ $\beta = 0.003$ $k = 27.3\times10^{-3}$ $\upsilon = 1.8\times10^{-5}$ $Pr = 0.72$ $C = 0.15$ $n = 1/3$ $l = 0.47$ $h = 6.5$	$T_s = 85$ $\beta = 0.003$ $k = 27.5\times10^{-3}$ $\upsilon = 1.8\times10^{-5}$ $Pr = 0.72$ $C = 0.27$ $n = 1/4$ $l = 0.47$ $h = 2.5$	$T_s = 35$ $\beta = 0.0033$ $k = 25.7\times10^{-3}$ $\upsilon = 1.58\times10^{-5}$ $Pr = 0.73$ $C = 0.59$ $n = 1/4$ $l = 0.68$ $h = 3.2$

As the HSBF tool is completely closed during the offline heating process, for calculating the internal heat convection coefficient, the internal space between the dies and heating platens was considered as rectangular enclosure and an h value of 2 W/m²C was determined for this condition in agreement with (Shabany, 2009). The governing equation that was applied to the case is:

$$Nu = 0.32(\frac{L}{H})Ra^{1/4} \quad with \quad Ra^{-1/4} \prec \frac{H}{L} \prec Ra^{1/4}, \quad h = \frac{Nu.k}{L} \tag{2.4}$$

where H and L are the dimensions of the enclosure. The validity of the above approach for the selection of the h values will be further confirmed based on the experimental and simulation results.

During the first step, the heating elements work with constant power of 2247 W/m² per heating element. This heat flux was assigned as the boundary condition in the numerical model.

However, during the second step the PID controller was acting and, therefore, the heat flux for each heating element was not constant and varied with time.

PID is a control system which calculates an error *e(t)* between a set-point (*sp*) and actual process variable (*pv*) and applies a correction based on PID terms.(Åström & Hägglund, 1995; Crowe et al., 2005). The maximum output of a PID controller is an adjustable value. In the present study in order to protect the heating elements, a maximum output of 90% was applied (i.e. nominal applied power to each heating element which will not go above 90 % of 3735 W).

During the experiments, the PID controller was functioning based on just one feedback from TC8, then the recorded temperature of the TC8 (as the controller TC) was used to calculate *e(t)*. At the early stage of the offline heating, due to significant difference between the target temperature and instantaneous TC8 temperature, the PID output is maximum. In accordance with the definition, *e(t)* was obtained as the difference between the target temperature and the actual temperature of the TC8 in every moment (470-*pv(t)*). Eventually the output of the PID were extracted as a curve and applied in the input heat flux of the heating elements. Fig. 2.4 shows the error and PID output.

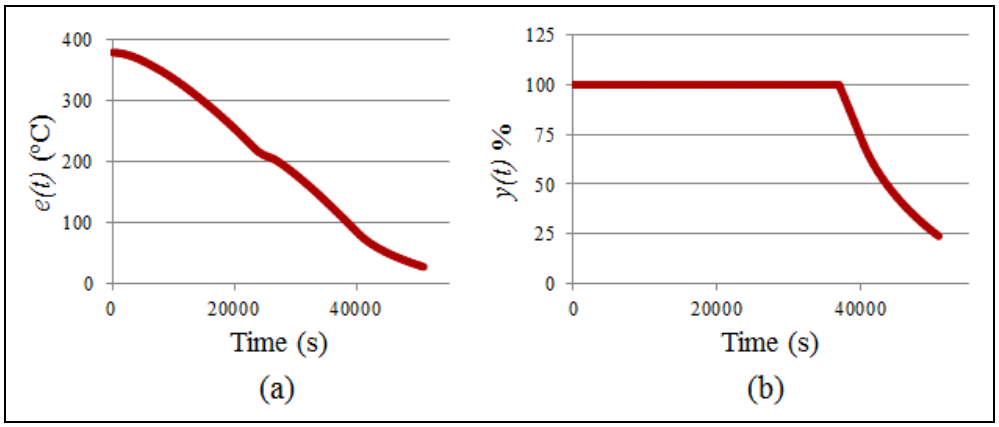

Figure 2-4 (a) error vs time (b) practical PID output

In practice, the heat input was set to increase step-wise with the specific percentages which are shown in Fig. 2.5. This recommendation is based on the heating rate of the die i.e. less than 60 ºC/hr in this case. Based on the PID output the power of heating elements is calculated and the result for each heating element is presented in Fig. 2.6.

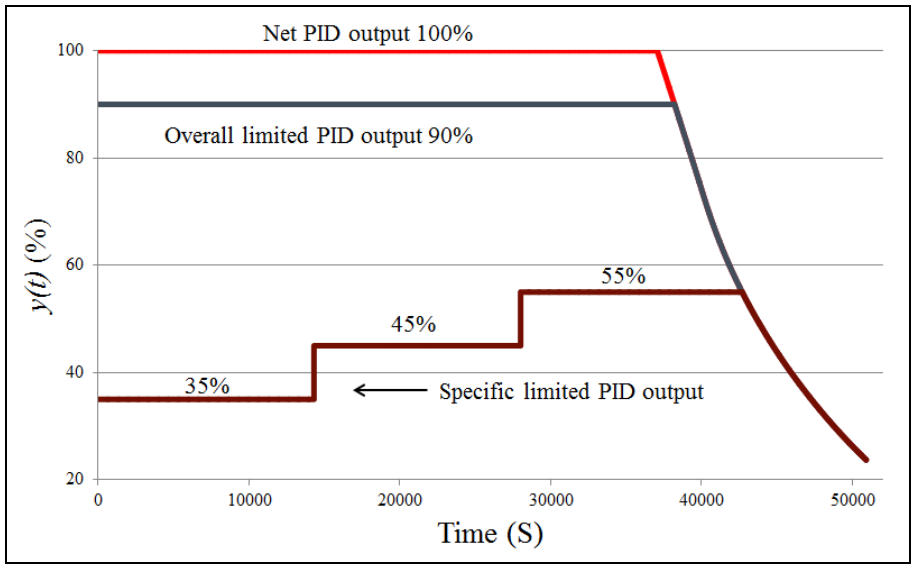

Figure 2-5 PID output during the second step of the offline heating process

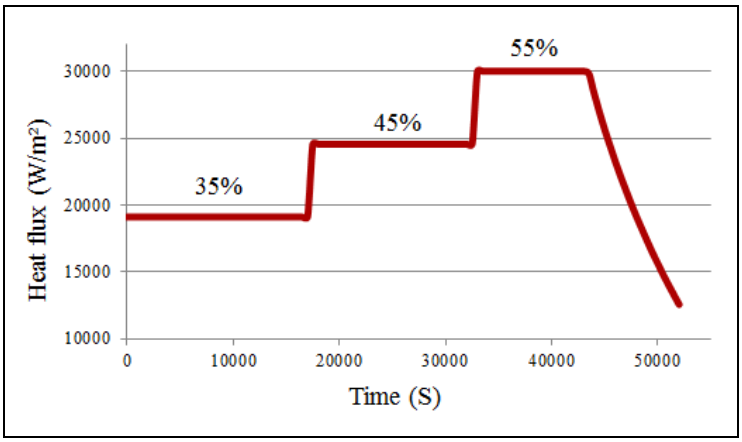

Figure 2-6 Power of the heating elements during the second step of the offline mode

2.4 Results and discussions

The variation of temperature with time for 8 thermocouples is presented in Fig. 2.7. As shown in this figure, the whole process takes near to 30 hours. At the first step the heating rate is very low which is normal according to the low applied power. At the second step the heating rate is considerably higher than that of the step one due to the higher applied voltage (600 V). The average temperature difference between the TCs at the end of the process is around 15 ºC. The predicted and experimental results for evolution of temperature during the offline test are compared in Fig. 2.8 for six TCs. In this figure, a stepwise PID output, i.e. 35, 45, and 55 %, was assumed in the simulation to maintain the maximum heating rate criterion that was less than 60 ºC/hour. There is a good agreement between the experimental and numerical results. The average of the temperature differences between the experiment and simulation during the entire process is 12 ºC which is reasonable. The temperature distribution at the end of the process is almost uniform with the maximum difference of 8 ºC on the surface of the die as presented in Fig. 2.9. In the heating and forming step of the HSBF process the temperature distribution of the blank follows the temperature distribution on the die surface. Temperature gradient within the part is one of the most important factors causing distortion in the HSBF final part, hence more the temperature distribution on the sheet material is uniform the probability of the distortion is less (S. Bikass, B. Andersson, A. Pilipenko, & H. P. Langtangen,

2012; Kessler et al., 2006; Totten, 2002). Thus, homogeneous temperature distribution on the surface of the die is desirable. In this case maximum 8 ºC difference is favorable which is obtained with considering all heating elements (whole area of the heating platens) as one zone. This result was expected because 1) the heating elements cover and heat all material of the die in a symmetric manner 2) the geometry of the die is almost symmetric 3) the distribution of the mass of the die is almost uniform. To have a better perspective and comparison, another simulation was done by adding TC11 as the second controller TC. The heating platens are divided to two zones while TC8 drives Zone 1 and TC 11 drives Zone 2 as depicted in Fig. 2.10. The target temperature for both TCs is the same as 470 ºC. The results in Fig. 2.11 show almost the same pattern of temperature distribution with the maximum difference of 12 ºC on the surface of the die. The comparison between these two cases suggests that considering all heating elements as one zone results more uniform temperature distribution on the surface of the die which is favorable. Moreover, considering just one zone for the heating elements could simplify controlling system while it decreases the cost of maintenance and repairing.

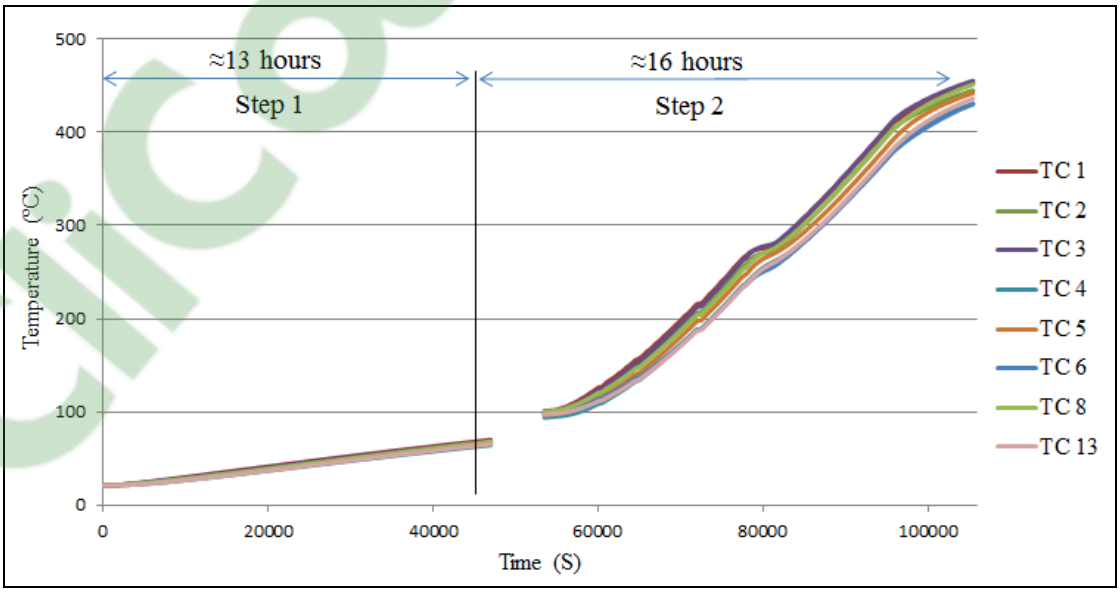

Figure 2-7 Experimental results for the offline heating experiment

It should be noted that, a lack of data acquisition occurred between the range of 47000 (S) to 53000 (S). This was due to an issue with the data acquisition software. Fortunately, this lack of data recording (1.5 hours over 30 hours) did not affect our analysis.

In this study the condition of the heating system gave the possibility to use just one controller TC to obtain the desirable temperature distribution. However, it should be noted that as the actual conditions deviate from the ideal ones, then the controller system will be more complex. For example, if the die is not symmetric or the distribution of the mass is not sufficiently uniform, then there should be more controller TCs to drive the system. In order to obtain more information on the mass distribution uniformity in the die and the position of the heat sources, the distance of the different points of the surface of the die from the heating plate (where the heating elements are installed) was calculated and it was found that the maximum difference was approximately 14 cm. This calculation suggests with an almost symmetric die and symmetric position of heat sources the 14 cm deviation in mass distribution could result in a uniform temperature distribution on the surface of the die and therefore only one controller TC would suffice.

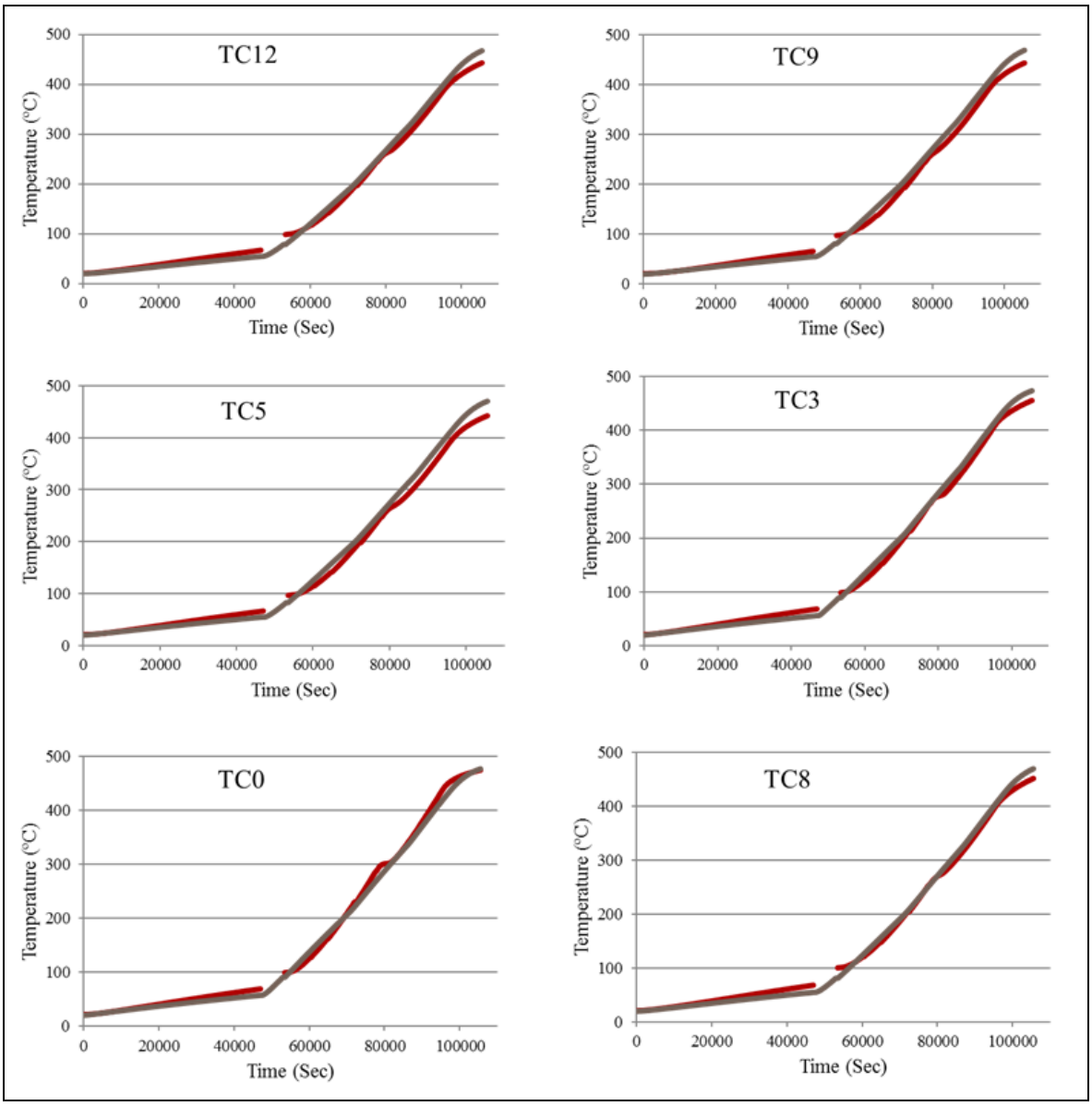

Figure 2-8 Comparison of the experiment and FEM results in the TCs

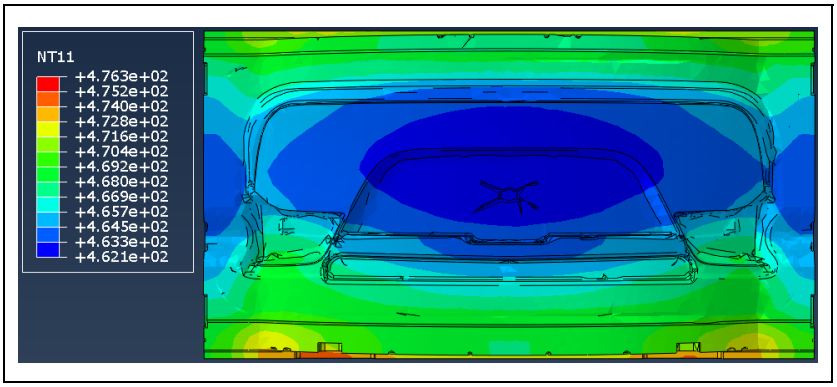

Figure 2-9 Temperature distribution on the surface of the HSBF die at the end of the offline heating process

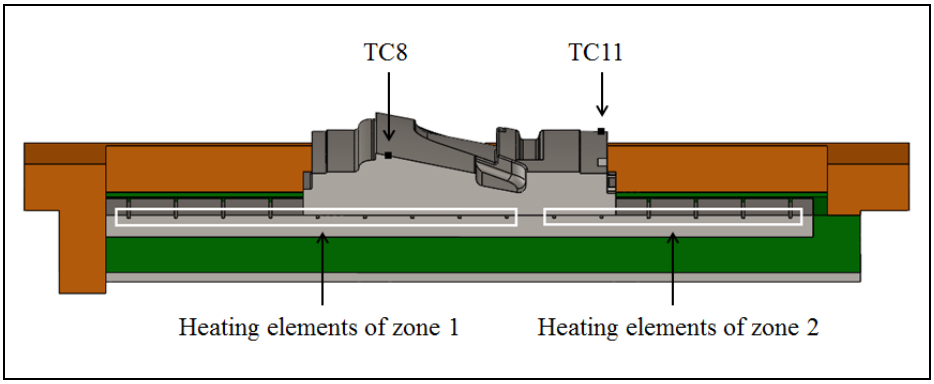

Figure 2-10 The divided heating platen to two zones

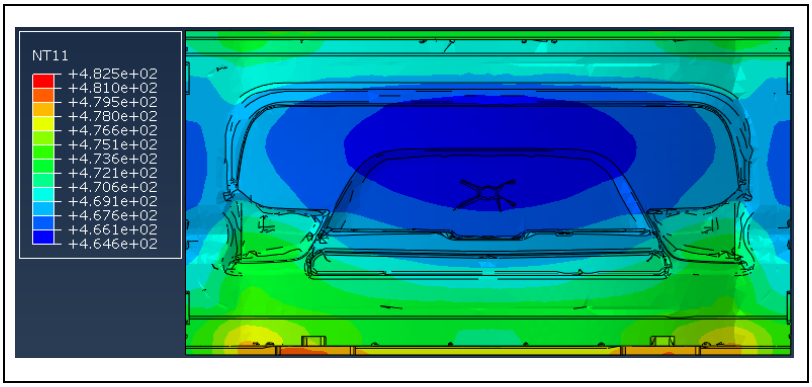

Figure 2-11 Temperature distribution on the surface of the HSBF die at the end of the offline heating process with considering 2 PID controllers

As mentioned above the application of the step wise mode was with the objective to respect the maximum heating rate of less than 60 ºC/hour. It must be noted that the measured temperatures are those at the surface of the die not the whole die. However, numerical results show that the temperature evolution inside the die is similar to that at the surface. As illustrated in Fig. 2.12, the temperature evolution of TC12 and three selected points within the thickness of the die, obtained by simulation, follow nearly the same patterns. Thus it could be suggested that the heating rate of the points on the surface of the die would be an acceptable estimation for the heating rate of the bulk of the die.

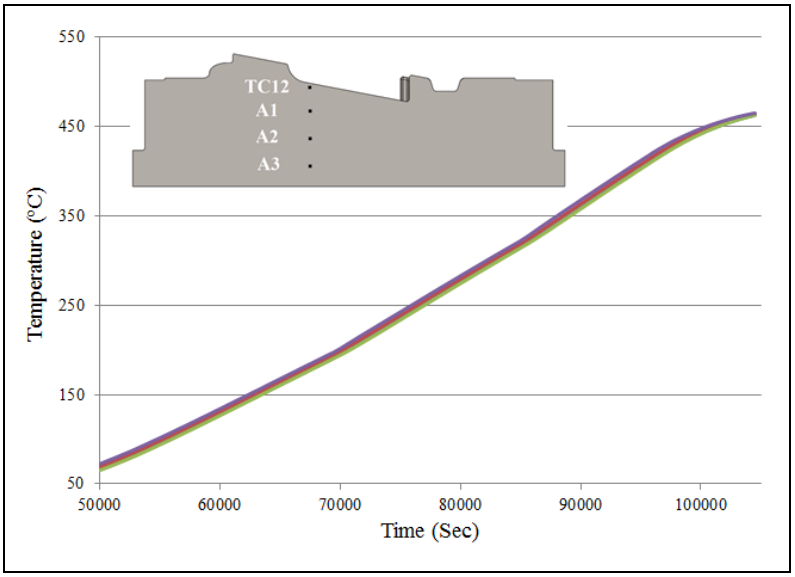

Figure 2-12 The temperature evolution comparison between TC12 and the points inside the die as A1, A2 and A3.

The results reported in Fig. 2.13 also show that the actual heating rate of the die is approximately 28º C/hour. Since the heat equation ($\dot{q} = mc\dot{T}$) assumes a linear relationship between the heating rate and $\dot{q}$ (power/wattage of heat source), then the PID adjustment could be directly correlated to the heating rate. In other words the ratio of the maximum to the actual heating rate, i.e. 60/28 in this case equals to that of PID percentage (i.e. input power). As the

average applied step wise power during the second stage (Fig. 2.7) was 45 %; therefore, multiplying 45 % by 60/28 indicates (≈95 %) that it is possible to use the 95% constant power.

Based on the above analysis and safety of the heating elements and the die, simulations were run with a constant 80 % power applied throughout the second stage of heating, instead of the step-wise heating, as shown in Fig. 2.13. With this assumption, the temperature evolution was simulated and the results are reported in Fig. 2.14. Results show that up to 7 hours could be saved from the overall offline heating period with the application of the new heating procedure. It should be mentioned that, the maximum heating rate criterion of less than 60 ºC/hour is also respected in the proposed approach. This achievement can give a good estimation for the heating requirement and determining the power of heat sources as heating elements in this case.

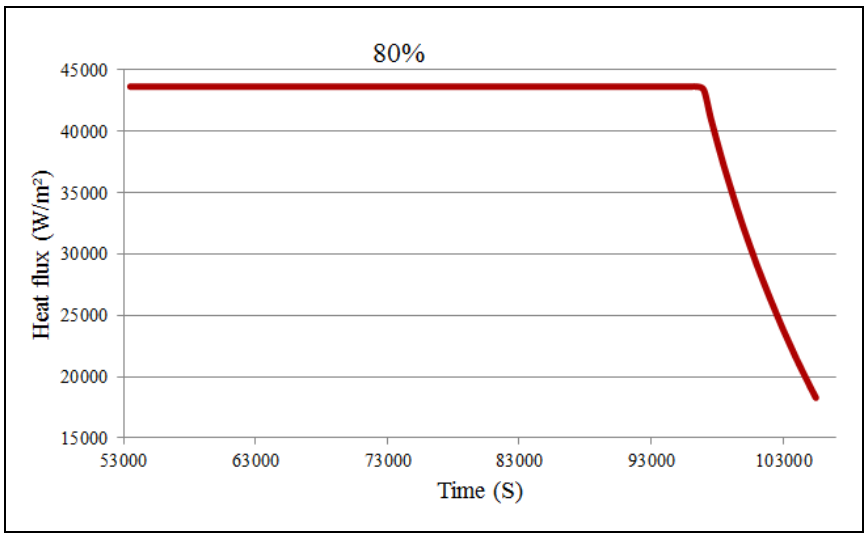

Figure 2-13 Full power of the heating elements during the second step of the offline mode

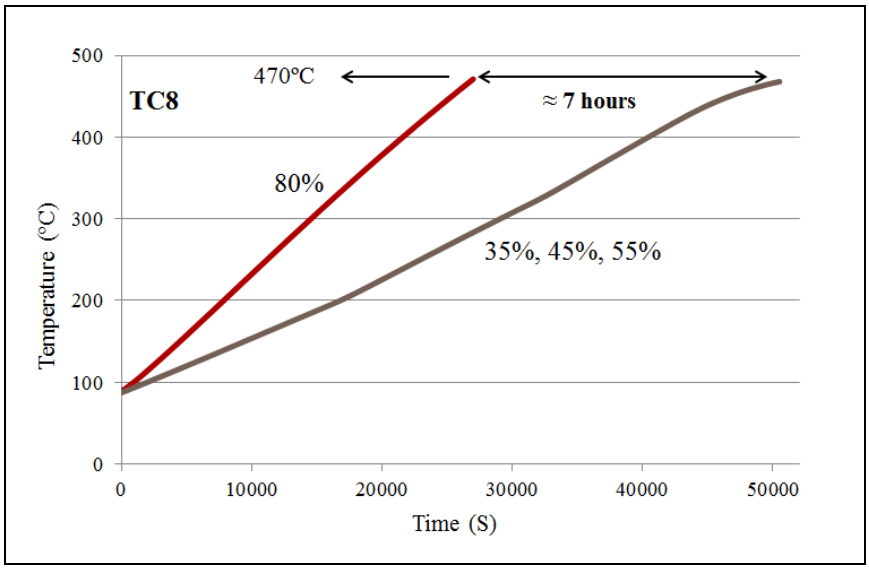

Figure 2-14 Comparison of the results between overall and specific limited PID output in the second step of the offline heating process

As mentioned in section 3, an *h* value of 2 W/m² ºC was assumed for the interior space of the HSBF tool. Although the calculation of the *h* value in an enclosure is a complex process; however, as reported in Fig. 15, based on the developed FEA model, if the internal convection is eliminated (i.e. *h*=0), a maximum difference of 5 ºC occurs at the end of the heating process which indicates that the effect of internal convection could be considered negligible in the present study. The above findings also show that considering all surfaces around the HSBF tool as a plate to calculate the external *h* value was a valid assumption.

With the above obtained results, it could be reasonably said that by considering the suitable assumptions and boundary conditions (as discussed above), the FE simulation allows obtaining an acceptable preliminary estimation of temperature distribution on the surface of the HSBF die.

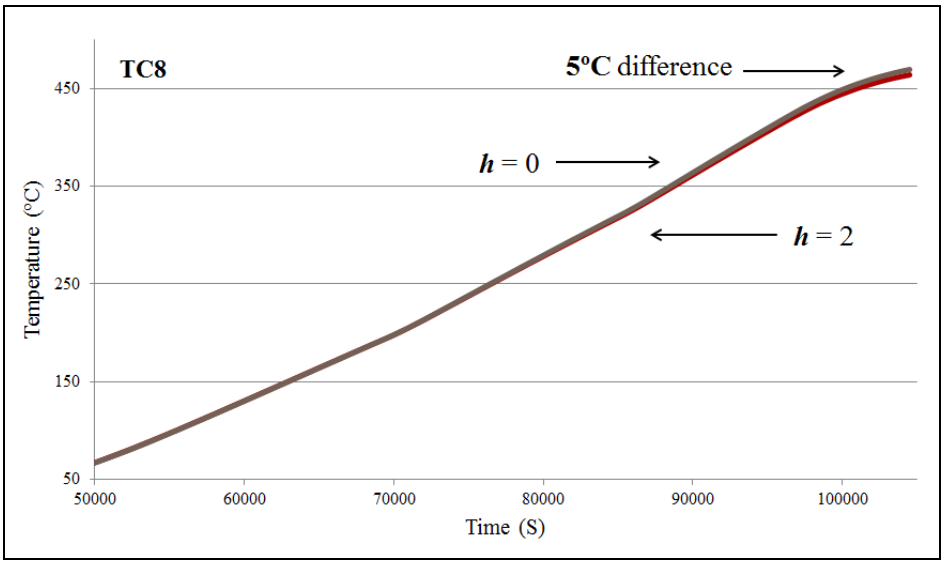

Figure 2-15 Comparison of temperature evolution in TC8 during the offline heating process with ***h***=0 and ***h***=2

2.5 Conclusion

1) The offline heating process of the HSBF tool was successfully simulated using finite element analysis and good agreements were obtained between the numerical and experimental results.

2) The measured heating rate at the surface of the die is a good representative of the heating rate inside the bulk of the die. Based on this result the obtained heating rate from the thermocouples was correlated to the power of the heat source.

3) The results showed that considering all heating elements of the HSBF tool as one zone resulted in more uniform temperature distribution in comparison to the case where the heating elements are divided into two zones.

4) The FEA showed that considering all surfaces around the HSBF tool as plates was a reasonable simplifying assumption for the calculation of the external *h* value and the internal convection heat transfer during the offline heating process in the HSBF tool is a negligible phenomenon.

CHAPTER 3

FINITE ELEMENT AND EXPERIMENTAL ANALYSIS OF THE COOLING STAGE OF SUPER PLASTIC FORMING PROCESS

Alireza Aleyari[a], Nicolas Bombardier[b], Xuan-Tan Pham[a], Mohammad Jahazi[a]

[a] Department of Mechanical Engineering, École de Technologie Supérieure (ETS), Montreal, QC, H3C 1K3, Canada

[b] Verbom Inc., 3820 boulevard Industriel, Sherbrooke, QC, J1L 2V1, Canada

Paper submitted to the journal of *Materials Engineering and Performance* In April 2020

Abstract

Super Plastic Forming (SPF) is a developed manufacturing method in which a superplastic thin sheet metal could be extended to very large strains (200 % to 1000 %) and deformed to a complex shape. One of the major challenges in this technique is the control of temperature during the process as it has a significant impact on the distortion of the final product. This study is aimed to experimentally and numerically analyze the temperature evolution during the cooling stage of the SPF process. In this regard, an industrial scale SPF product made of thin sheet 5083 aluminum alloy was instrumented with 9 thermocouples (TCs) attached at different locations of the part and the temperature evolution was recorded. The process was numerically simulated with the commercial Finite Element Analysis (FEA) software ABAQUS with a new approach which considers local temperature evolution during the process. A good conformity between the numerical and experimental results was obtained confirming the validity of the assumptions on heat transfer conditions.

Keywords: Super plastic forming, Cooling, Heat transfer coefficient.

3.1 Introduction

Heat treatment is one of the most common processes that takes place in different industrial applications and cooling as the last step in any heat treatment process has a significant impact on the final mechanical properties and dimensional characteristics of a part (Rajan, Sharma, & Sharma, 2011). In the thermal analysis of a cooling process, Heat Transfer Coefficient (HTC) is one of the most important parameters that should be considered; particularly, when it comes to the prediction of temperature evolution using numerical simulation. However, accurate determination of the HTC is challenging when it comes to advanced manufacturing processes such as Super Plastic Forming (SPF) where large thin sheet material is formed into complex shapes.

In the SPF process, a fine grain material (average grain size between 5 μm and 15 μm) is deformed to very large elongations (sometimes up to 1000 %) at high temperature (0.4 - 0.6 of melting temperature) and very low strain rates (around 10^{-3} s^{-1}). SPF has been successfully used in automotive and aeronautic industries although the low strain rate that results in high production cycle time is the weakness of the method for the mass production scale (Gillo Giuliano, 2011; Majidi et al., 2018b). Fig. 3.1 depicts schematically the three main steps in a SPF process, consisting of heating the sheet material, which could be performed out of the die, blow forming with an inert gas, and cooling.

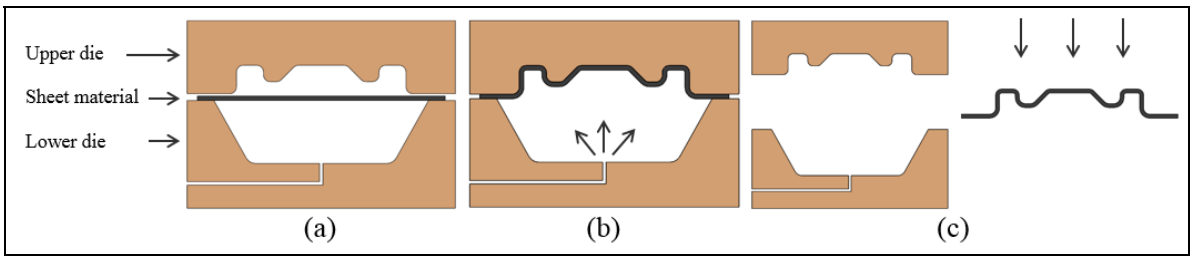

Figure 3-1 The schematic of the SPF technique a) Heating of the sheet material, b) Gas blow forming, c) Cooling

Due to the complex thermomechanical process, the final part could suffer from thinning, wrinkling, distortion, and cavitation that could arise during the entire process (Cappetti et al., 2010; Kuppuswamy Anantha Padmanabhan, Vasin, & Enikeev, 2012; Tan, Liew, & Tan, 2007; Tang, Fuh, & Lee, 2015). Up to now, most of the investigations in the SPF process have focussed on the material behavior and formability (Balasubramanian, Stalin, Ramanathan, & Ravichandran, 2019; Kumar, Ismail, Vijayarasi, & Kumar, 2019; Majidi, Jahazi, & Bombardier, 2018a; Majidi et al., 2019; Nazzal, Khraisheh, & Darras, 2004; Vijayananth, Jayaseelan, & Kumar, 2019), while less attention has been paid to other aspects of the process, such as thermal analysis, SPF press and tool quality, etc.

For example, Sorgente et al. (Sorgente et al., 2016) examined the feasibility of conducting the SPF process using common industrial presses. Velay et al. (Velay et al., 2008) studied the thermomechanical loading of a SPF tool in order to improve the tool lifetime. Mauduit et al. (Mauduit et al., 2017) reported on the application of infra-red (IR) lamps to heat up the sheet material during the SPF process. Mis et al. (Mis et al., 2013) investigated the effects of temperature variations and the state of heat transfer on the quality of the final product during the SPF process. Rollin et al. (Rollin et al., 2016) investigated the distortion problem in a SPF part.

However, while all SPF parts are cooled after the forming stage and temperature variations during the cooling stage could induce changes in the final shape of the SPF products, very little information is available in this field. Specifically, because of the thin and large body of SPF parts, the cooling condition is different from the common quenching processes and if not well controlled, the SPF parts suffer from distortion which results in rework and sometimes rejection. Thus, understanding of the temperature evolution and the thermal analysis of the cooling process is essential. In this regard, this work presents a thermal analysis of the cooling stage of the SPF process. A combination of numerical and experimental analyses was used to study the temperature evolution during the cooling stage considering that all modes of heat

transfer (conduction, convection, and radiation) take place during the cooling. A new approach is proposed for the determination of the HTC and the proposed methodology is then applied to simulate temperature evolution during the cooling process of an industrial size part and then experimentally validated under real working conditions.

3.2 Heat transfer analysis

The cooling stage of the process begins when the part is ejected from the SPF die. For the simulation of the temperature variations during the cooling process, the initial temperature distribution of the part is required. In practice, this means that the temperature variations within the bulk of the SPF tool should be simulated and validated. Then, the temperature distribution on the surface of the die at the ejection time is used as initial temperature distribution of the part at the beginning of the cooling stage. On the other hand, as the HTC is a temperature dependent variable and the temperature distribution at the beginning and during the cooling process is not in reality uniform, then the HTC should be calculated for each point of the part, which is a lengthy and time-consuming process. In this regard, a new approach based on local temperature variation is proposed and will be detailed below.

For the simulation of the temperature and heat transfer during the cooling stage, the part was divided into 9 zones with equal dimensions (0.48 m×0.63 m). A temperature value was considered for every zone from the beginning of the cooling stage and the HTC was calculated based on the temperature evolution of each zone. The validity of this assumption will be discussed further in section 5. Figure 2 depicts the configuration of the SPF part with the nine zones. It must be noted that the actual part has small protrusions, with a height of about 12 mm, on its surface, as shown in Fig. 3.2; however, they were neglected for simplification purposes in the calculations, and the part was considered as a flat panel.

Figure 3-2 The divided SPF part into 9 equal zones

3.3 Experimental procedure

The material used in this investigation was the aluminum alloy AA5083 with the nominal composition shown in table 3.1 and the physical properties at different temperatures, presented in table 3.2.

Table 3-1 Composition of the SPF part (Davis, 1993)

Element	Fe (max)	Si (max)	Cu (max)	Mn	Mg	Cr	Zn (max)	Ti (max)	Others (total)
Wt (%)	0.4	0.4	0.1	0.4-1	4-4.9	0.05-0.25	0.25	0.15	0.15

Table 3-2 Physical properties of the SPF part

	@ 20 ºC	@ 100 ºC	@ 200 ºC	@ 300 ºC	@ 400 ºC	@ 500 ºC
Thermal conductivity (k) (W/m ºC) (Summers et al., 2015)	125	135	145	155	165	170
Specific heat (C_p) (J/kg ºC) (Summers et al., 2015)	920	930	960	1010	1050	1100
Density (ρ) (kg/m³) (Totten & MacKenzie, 2003)	2670	-	-	-	-	-

The dimensions of the SPF part was 1.9 m×1.44 m×0.0024 m with the geometry presented in Fig. 3.3.

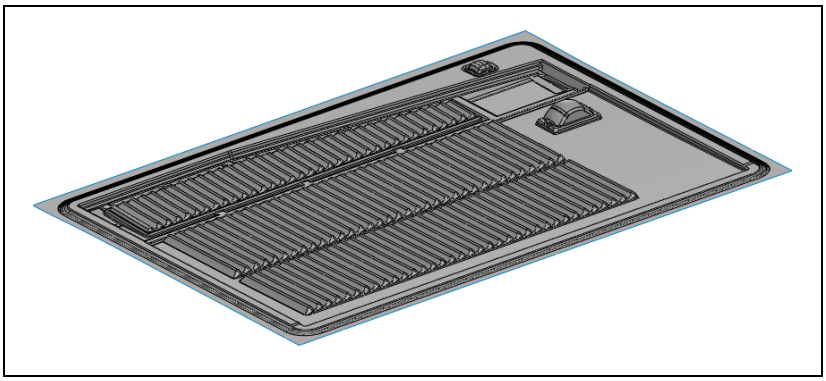

Figure 3-3 The CAD model of the SPF part

Temperature measurements were performed on the actual production line of the SPF part. To this end, a K type thermocouple (TC) was attached at the center of each zone for simultaneous measurement of temperature in the nine locations. The part was then placed on the running SPF tool between the upper and lower SPF dies. After reaching the target temperature (≈470 ºC in this case) the ejecting process was triggered and the part was removed out of the press

on a carrier. Two rows of fans that covered the entire surface of the part were used to cool down the part at the exit of the press. A data logger was used to record the temperature at every second during the entire cooling process for each of the nine TCs. Table 3.3, displays the initial temperature at the center of each zone at the start of the cooling process.

Table 3-3 The initial temperature of the different zones of the part at the beginning of the cooling stage

TC1	TC2	TC3	TC4	TC5	TC6	TC7	TC8	TC9
444 ºC	448 ºC	444 ºC	459 ºC	468 ºC	462 ºC	450 ºC	450 ºC	448 ºC

3.4 Numerical model and boundary conditions

For the numerical simulation, ABAQUS 6.13 was used and the part was meshed with more than 37000 3-node triangular shell elements. All heat transfer modes (conduction, convection, and radiation) during the cooling stage were considered in the analysis and the required physical properties of the part as reported in table 2 were used in the simulations. It should be mentioned that, the variation of the density (ρ) of the alloy was considered negligible within the range of the working temperatures. Furthermore, an emissivity value of 0.1 was assigned for the surface of the SPF part.

During the cooling stage, the top side of the part was exposed to the blowing fans and the bottom side faced with the carrier. Thus, a forced convection condition was assumed for the top side of the part and a natural one on the bottom surface. Moreover, radiative heat transfer took place between the part and the ambient medium as well as with the carrier, while conduction occurred within the part and on the contact points with the carrier. For the calculation of the HTC, every zone was considered as an independent entity and all heat

transfer modes were taken into account. Fig. 3.4 summarizes schematically the heat transfer modes of a zone during the cooling process.

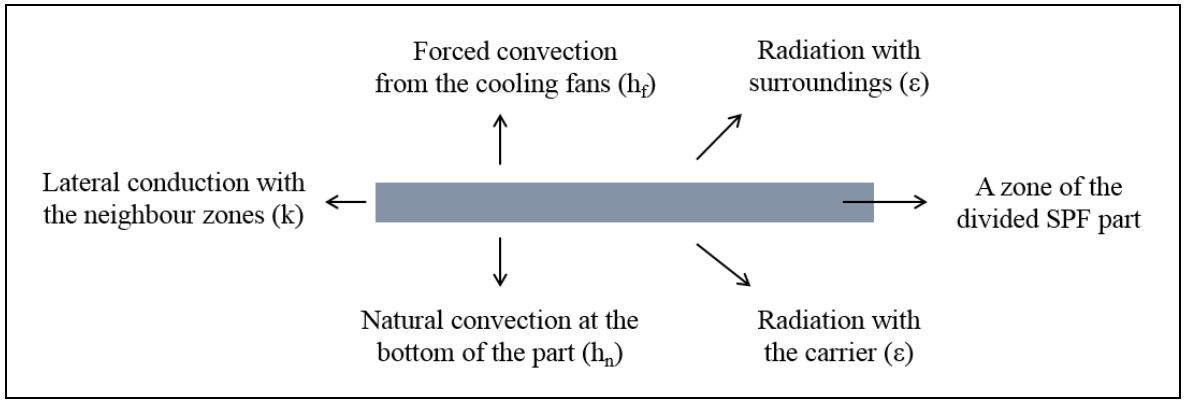

Figure 3-4 Heat transfer modes occuring in a zone during the cooling process of the part

The energy balance for every zone could be written as:

$$\dot{q} = 2\sigma\varepsilon A(T_s^4 - T_\infty^4) + h_f A(T_s - T_\infty) + h_n A(T_s - T_\infty) + kA_l \frac{dT}{dx} \qquad (3.1)$$

where $\dot{q}$ is the heat transfer rate (W), σ is the Stefan Boltzmann constant (W/m² K⁴), ε is the emissivity of the part, T_s is the surface temperature (ºC), T_∞ is the ambient temperature (ºC), h_f is the forced convection coefficient (W/m² ºC), h_n is the natural convection coefficient (W/m² ºC), k is the thermal conductivity of the part (W/m ºC), A is the area of the zone (m²), and A_l is the area of the lateral surface of the zone (m²).

As the SPF part is thin, the lateral surfaces are very small in comparison with the top or bottom ones. Therefore, it is reasonable to assume that heat transfer between the zones has a negligible influence on the temperature changes of the part. Thus, the last term in equation 3.1 could be eliminated and from there the heat loss between the times t_1 and t_2 (q) can be determined by:

$$q = \int_{t_1}^{t_2} [2\sigma\varepsilon A(T_s^4 - T_\infty^4) + h_f A(T_s - T_\infty) + h_n A(T_s - T_\infty)]dt \quad (3.2)$$

The HTC was directly calculated from the experimental cooling curves in agreement with the approach employed by other authors (Liščić, 2016; Zhang et al., 2013). As the cooling of the SPF part is not classified as a fast cooling process (i.e. quenching); therefore, the HTC is not expected to be as high as in the quenching process, then it is important to know the contribution from the radiation heat transfer. In this regard, the radiative heat transfer was independently taken into account in the analysis.

When using experimental cooling curves for the calculation of the HTC, it is critical to have an accurate estimation of the internal heat conduction. When internal conduction is present, usually inverse method is used to calculate the HTC (Huiping et al., 2006; Xu, 2006). The criterion of the Biot number of the process indicates whether or not it is necessary to consider the internal conduction for the calculation of the HTC. The Biot number is expressed as:

$$Bi = \frac{hL_c}{k} \quad (3.3)$$

where h is the heat convection coefficient (W/m^2 ºC), k is the thermal conductivity (W/m ºC) and L_c is the characteristic length (m). If the Biot number is equal or less than 0.1, then the contribution from internal conduction could be considered as negligible in the calculation of the HTC. In other words, this implies that the instantaneous temperature throughout the zone could be considered as uniform (Holman, 2008). In the present case, due to the dimensions of the part, specially, its small thickness, the Biot number is less than 0.002, indicating a negligible contribution of the internal conduction to the overall heat transfer during the cooling stage of the part. The above analysis provides a reasonable justification for the assumption made to consider uniform temperature in each zone.

The heat loss by the part between times t_1 and t_2 can be written as below:

$$q = mc(T_{t_2} - T_{t_1}) \tag{3.4}$$

Where q is the heat loss (J), m is the mass (kg), c is the specific heat (J/kg ºC) and T is the temperature at the given times t_1 and t_2.

If the heat convection coefficient between the times t_1 and t_2 is considered as constant, then equations 3.2 and 3.4 could be equated:

$$mc(T_{t_2} - T_{t_1}) = -[2\sigma\varepsilon A(T_s^4 - T_\infty^4) + h_f A(T_s - T_\infty) + h_n A(T_s - T_\infty)](t_2 - t_1) \tag{3.5}$$

Then, the total heat convection coefficient can be determined as:

$$h_{total} = h_f + h_n = -\frac{mc(T_{t_2} - T_{t_1})}{A(t_2 - t_1)(T_s - T_\infty)} - \frac{2\sigma\varepsilon(T_s^4 - T_\infty^4)}{(T_s - T_\infty)} \tag{3.6}$$

In the calculation of the *h* value, the T_s was considered equal to the $(T_{t1}+T_{t2})/2$.

For the calculation of the radiation heat transfer, the position of the SPF part during the cooling process was considered. As shown schematically in Fig. 3.5, at the early stage of the cooling process, the SPF part exchanges radiative heat with the upper die, surroundings and the carrier.

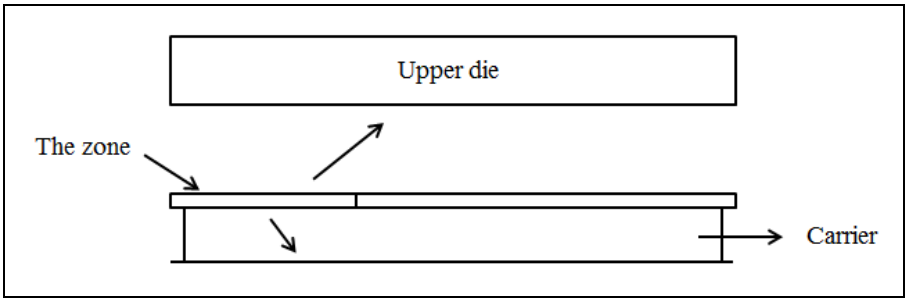

Figure 3-5 Schematic representation of the radiation heat transfer exchange between the SPF part and the surroundings.

In this position, the part has almost the same temperature as the upper die, therefore, no radiation heat transfer between the upper die and the part was assumed for the calculation. On the other hand, as the temperature of the carrier did not increase considerably during the cooling process, the radiation as well as conduction heat transfer exchange between the part and the carrier was estimated negligible. Therefore, only radiation exchange with the ambient air was considered in the numerical simulation.

3.5 Results and discussions

The temperature variations with time for the 9 zones of the SPF part during the cooling stage is illustrated in Fig. 3.6. The maximum temperature difference between the zones occurs after about 145 seconds with 54 ºC between Zones 3 and 8 while it is 6 ºC at the beginning of the process. The maximum difference at the beginning of the process is 24 ºC between Zones 3 and 5. The figure also shows that the rate of cooling decreases with time, which indicates the dependency of the cooling rate to the temperature. It is also important to note that a sharp temperature decrease is observed in the first 150 seconds. After this stage, temperature variations keep a smoother pattern until the end of the cooling process.

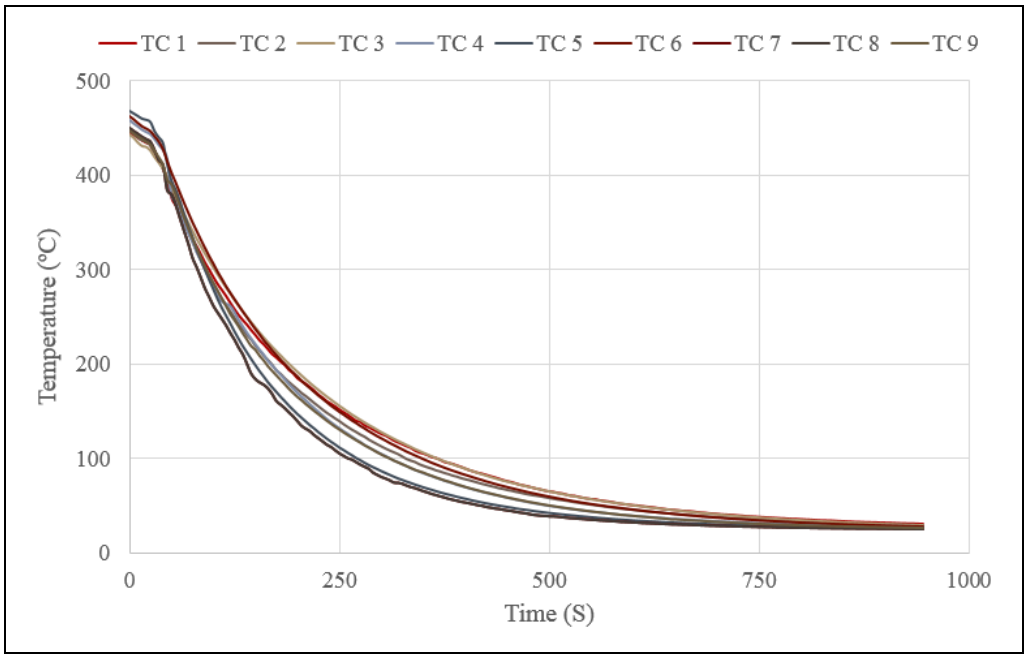

Figure 3-6 Temperature evolution for the different zones of the SPF part during the cooling stage

In order to have a better perspective about the temperature variation in different zones, cooling curves of Zones 3 and 5 are shown in Fig. 3.7. As the figure shows, the temperature of Zone 3 is higher than that of Zone 5 at the beginning but after about 70 seconds, it becomes lower and remains so until the end of the process. The faster cooling of Zone 5 indicates that its HTC is higher compared to that of Zone 3, at least for a large part of the cooling process. This aspect will be discussed in more details in the next section.

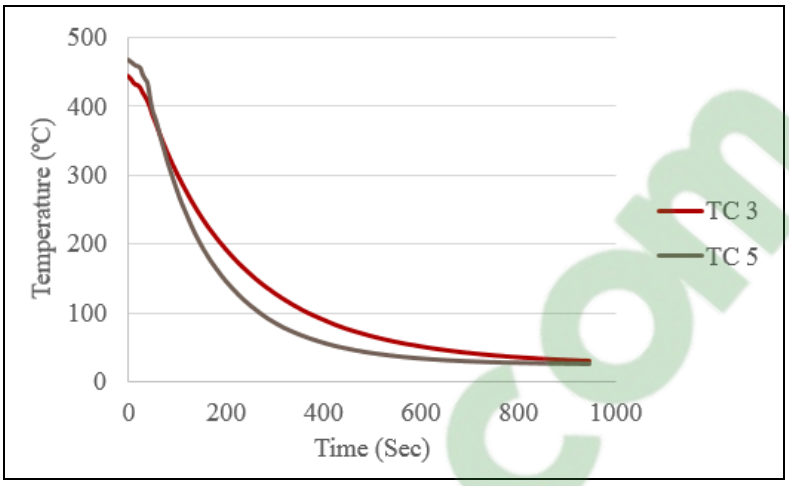

Figure 3-7 Comparison of the temperature evolution for Zones 3 and 5 during the cooling stage

Using the above experimental measurements and equation 3.5, the convection heat transfer coefficient was calculated for each zone and some illustrative examples for Zones 1, 2, 5, and 6 are presented in Fig. 3.8. As the figure shows, the *h* values in the above mentioned zones have similar patterns but different values. At the beginning of the cooling process, the general pattern is that, *h* has low values then reaches a maximum value followed by a descending trend until the end of the process. The low values at the beginning (about the first 50 seconds) indicate that the part is under the upper die and not submitted to the flow of the cooling fans and the highest values occur when the part stands under the blowing fans.

It must be noted that, for the calculation of the heat convection coefficient, a time interval (t_2-t_1) of 5 seconds was considered and the experimental cooling curves were directly used. Therefore, the determination of the HTC could be considered as a direct method thereby increasing its reliability. Based on the obtained results, the average *h* value for each zone was determined to be approximately 30 W/m^2 ºC. These values are significantly lower in comparison with those obtained in liquid quenching processes where HTCs are sometimes two hundred times higher (Yang et al., 2013).

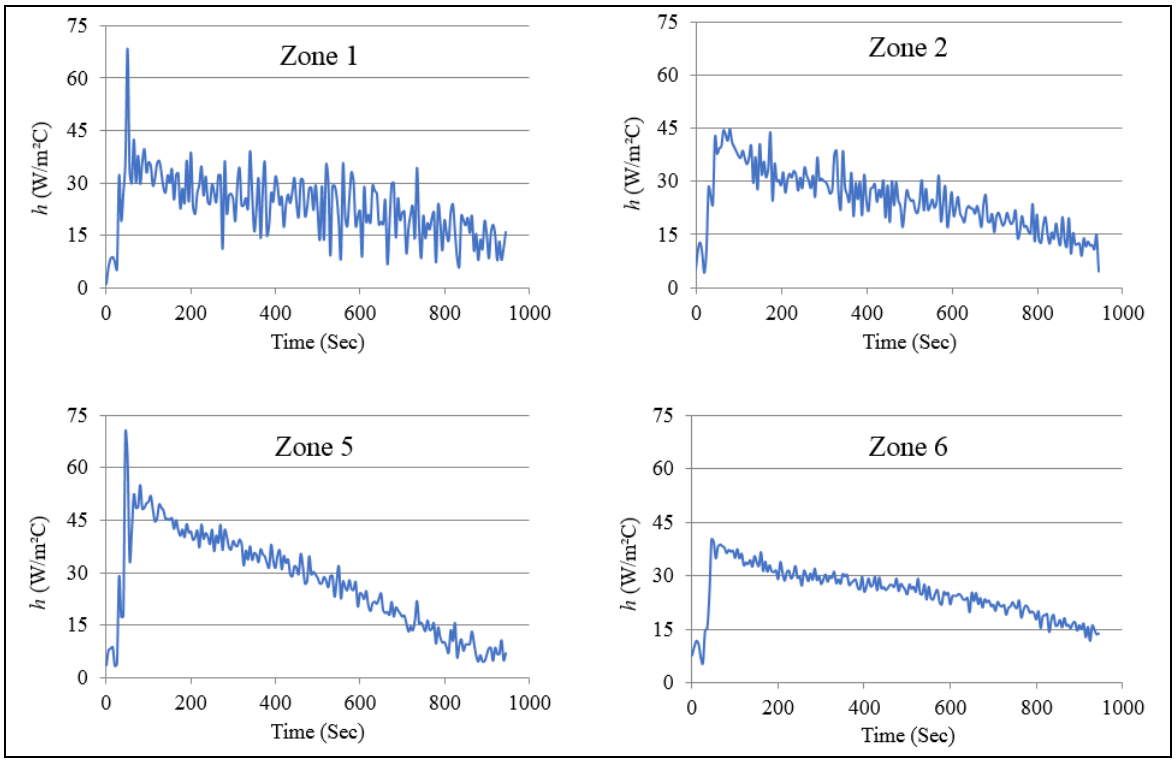

Figure 3-8 The heat convection coefficient variations during the cooling stage

The fluctuation in the *h* values reported in Fig. 3.8 curves are related to the variabilities associated with thermocouple readings and has also been observed by other authors (Kim & Oh, 2001). Indeed, in the calculation of the *h* value the term (T_{t2}-T_{t1}) appears in the equation and is used for the calculation of the expanded form of the cooling rate. In some cases, a curve-fitting is applied on the cooling curves and eliminate the fluctuations in the cooling rate and *h* value curves (Xiao et al., 2011). In the present work, both the raw data and smoothing ones were used for the calculation of the *h* value. For the smoothing of the cooling curves, a sixth-order polynomial was applied and the curve-fitted cooling evolutions were determined as illustrated in Fig. 3.9 for the data related to Zone 5. Using the smoothed cooling curves, the evolution of the *h* value during cooling was calculated for Zones 5 and 6, and the results are presented in Fig. 3.10. As the figure shows with using the temperature data from the smoothed cooling curves, the fluctuation is completely removed.

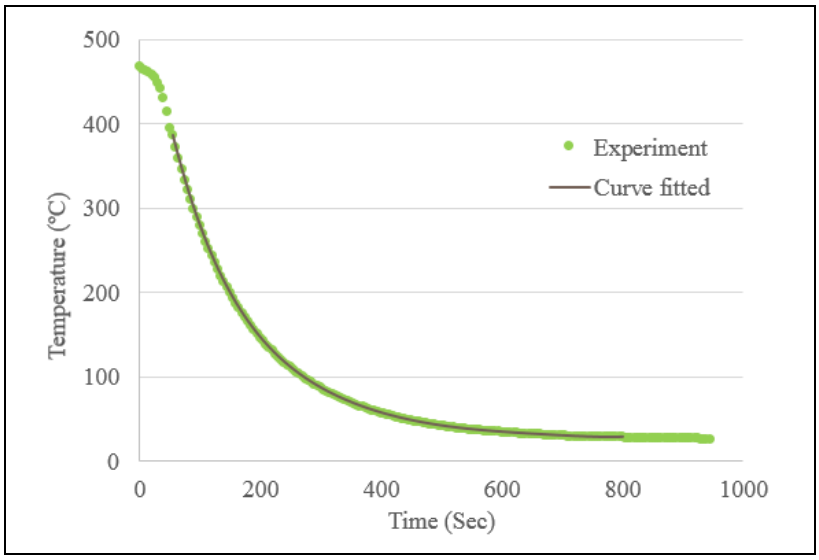

Figure 3-9 Comparison of the smoothed cooling curve with the origin one in Zones 5

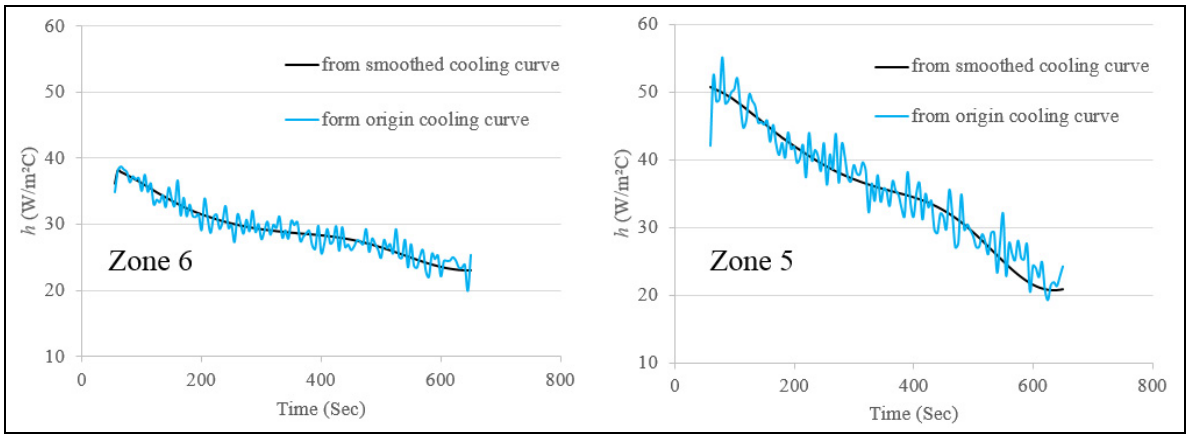

Figure 3-10 Comparison of the *h* values determined by the smoothed cooling curves and the origin ones in Zones 5 and 6

In the comparison between the temperature evolution of Zones 3 and 5, it was mentioned that the *h* value in Zone 5 is higher than that of Zone 3. Fig. 3.11 compares the *h* values of the two zones. As the figure shows, the *h* value in Zone 5 is more intensive until around 600 seconds where the temperature of both zones is below 70 ºC and it could reasonably considered that the cooling process is completed.

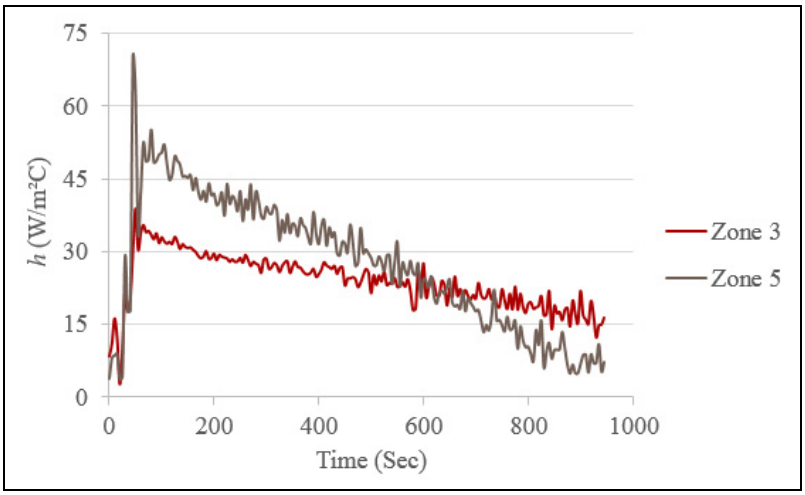

Figure 3-11 Comparison of the heat convection coefficient evolution for zones 3 and 5

In another comparison, the temperature evolution between zones 3 and 6 was considered. As Fig. 3.12 indicates, the temperature evolution of the two zones are close to each other, unlike the previous case. Although at the beginning the temperature of zone 6 is higher than that of zone 3, but during the process, they show very similar variations with time. This phenomenon could be explained by comparing their *h* values (Fig. 3.12b) where it can be seen that, the *h* value of both zones have very close values during the cooling cycle.

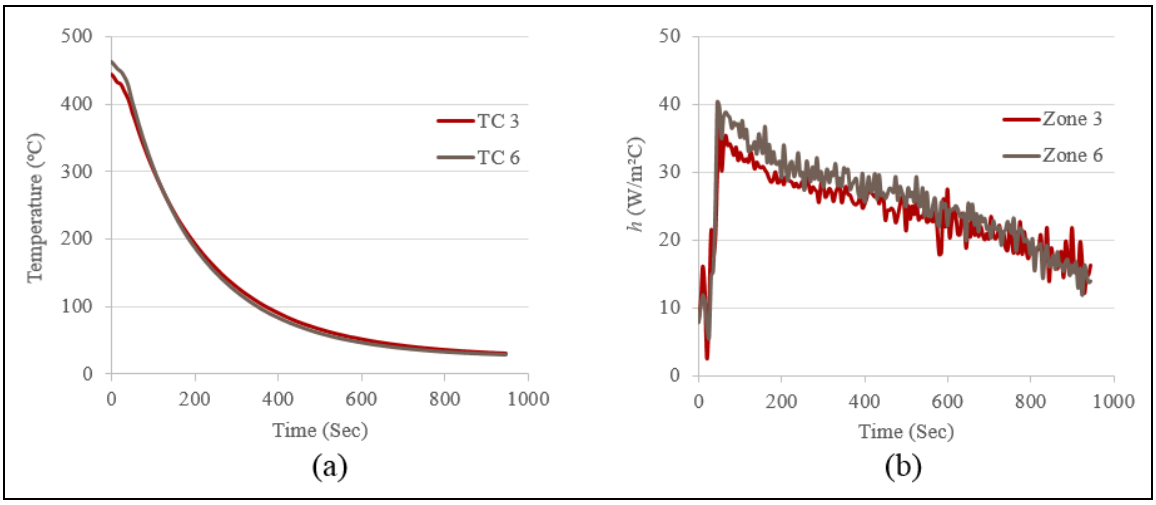

Figure 3-12 a) Temperature evolution b) Heat convection coefficient for Zones 3 and 6

The determined *h* curves for each zone were directly applied in the numerical simulation and the results are compared with the experimentally determined ones in Fig. 3.13. As indicated, there is a good conformity between the numerical and the experimental results. During the entire cooling process the maximum difference between the numerical and experimental results is in average about 9 ºC which occurs in the early stages of the process.

The above conformity supports the initial assumptions made regarding the division of the part in nine zones and assuming uniform instantaneous temperature in each of them. Furthermore, the obtained results confirm the validity of the assumptions regarding the negligible contributions from through thickness and lateral conductions to the *h* value. The approach has the significant advantage of requiring much shorter calculation cost and avoid modelling the whole SPF tool to find the initial temperature distribution of the part for the simulation of the cooling stage.

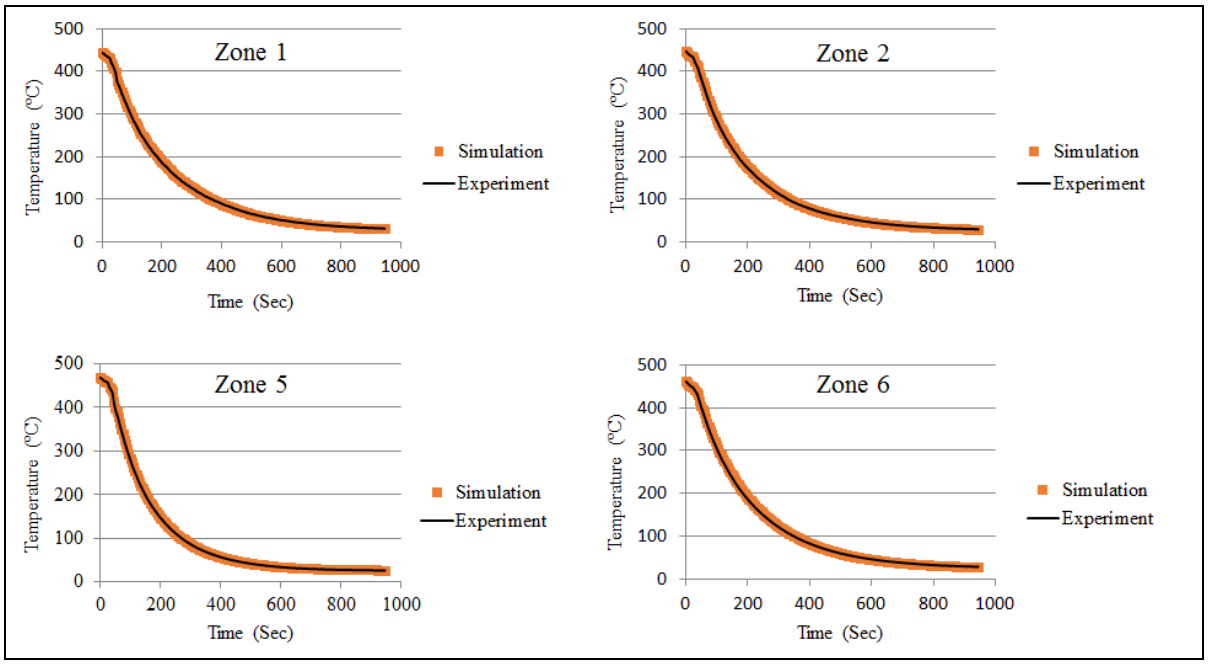

Figure 3-13 Comparison of the temperature evolution between the simulation and experiment

The impact of using in the simulations either *h* values obtained from raw cooling curve data or from smoothed cooling curves was evaluated. Illustrative results are presented in Fig. 3.14 for Zones 2 and 6. The obtained results indicate that both methods are reliable with a relatively better precision when the non smoothed data is used.

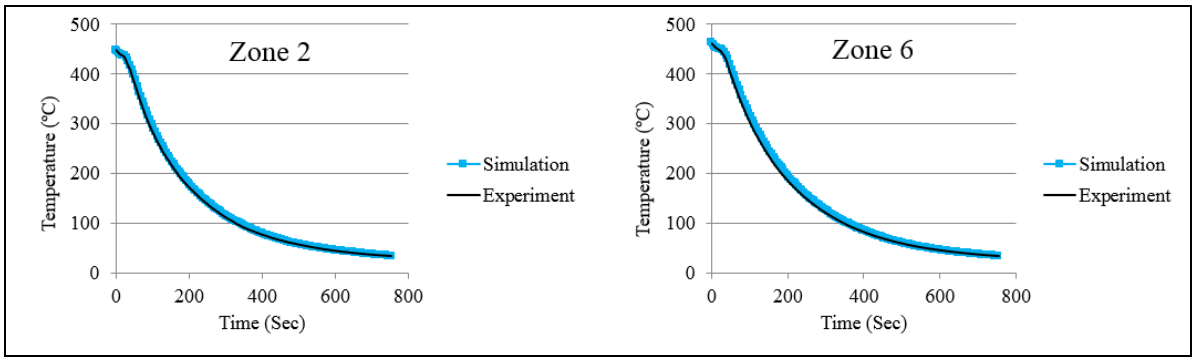

Figure 3-14 Comparison of the temperature evolution between the simulation and experiment based on the *h* values determined by the smoothed cooling curves

As discussed in section 4, in order to determine the contribution of the radiative heat transfer during the cooling process, the heat transfer rate for both radiation and convection modes were caculated and the result are depicted in Fig. 3.15. As shown, the average contribution of the radiation term is less than 5% of the total heat transfer rate. Although, the range of the heat convection coefficient during the air cooling process is much lower than the quenching process, it appears that the radiation term has a negligible contribution to the heat transfer process. Therefore, it could be suggested that in the cooling stage of the SPF process, with the determined range of the *h* values and the working temperature of this study, the contribution of the radiation term in the calculation of the HTC could be neglected.

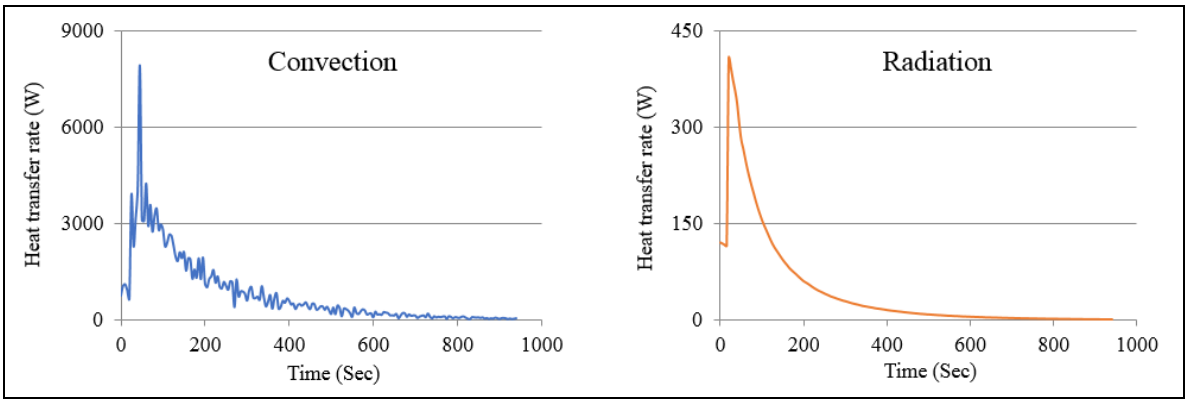

Figure 3-15 Comparison of the heat transfer rate between convection and radiation during the cooling process

3.6 Conclusions

1) Temperature evolution during the cooling stage of the SPF process was simulated using finite element method validated by experimental measurements.

2) A new approach was used to calculate the HTC values in different locations, which resulted in considerable reduction of the simulation time without affection the accuracy of the predictions.

3) *h* values calculated from raw cooling curve data or from smoothed cooling curves led to the same level of accuracy in the predictions.

4) Internal conduction and radiative heat transfer during the cooling stage of the SPF process have minor contributions to the overall heat transfer process.

CHAPTER 4

EXPERIMENTAL ANALYSIS OF THE DISTORTION IN THIN SHEET ALUMINUM ALLOY PARTS DURING THE COOLING STAGE OF SUPER PLASTIC FORMING PROCESS

Alireza Aleyari[a], Nicolas Bombardier[b], Xuan-Tan Pham[a], Mohammad Jahazi[a]

[a] Department of Mechanical Engineering, École de Technologie Supérieure (ETS), Montreal, QC, H3C 1K3, Canada

[b] Verbom Inc., 3820 boulevard Industriel, Sherbrooke, QC, J1L 2V1, Canada

Paper submitted to the journal of *Advanced Manufacturing Technology* In July 2020

Abstract

Super Plastic Forming (SPF), is an advanced manufacturing technique, used to form a thin sheet metal into complex shapes with large magnitude of strains. One of the most important technical challenges in this method is the distortion of the final product during the post forming cooling stage. The present study was aimed to experimentally analyze the cooling stage of the process for a large size SPF component. In this regard, the component made of a thin sheet aluminum alloy (5083) was instrumented with 9 thermocouples (TCs) attached at different locations and the temperature variation was recorded. Four cooling scenarios representing different thermal conditions were experimented. After each experiment, the part was fully scanned with a 3D scanner camera and a 3D surface model of every part was built. The model was then compared with the original CAD model of the SPF part with the 3D metrology

software PolyWorks. The results showed that more uniformity in the initial temperature distribution of the SPF part at the start of the cooling stage leads to less distortion of the part after cooling while more uniformity of the Heat Transfer Coefficient (HTC) did not show considerable effect on the distortion of the part.

Keywords: Super Plastic Forming, Distortion, Cooling, Heat Transfer Coefficient.

4.1 Introduction

Super Plastic Forming (SPF), is a well-known and established technology in the transportation industry for forming complex parts with large height to thickness ratios and uniform elongations up to 1000%. A combination of fine equiaxed grain material (few micro meters grain size), high temperature, between 0.4 and 0.6 of the melting point of the sheet material, and very low strain rates ($\approx 0.001\ s^{-1}$) are required for a successful SPF process. Despite the low strain rate, defects such as thinning, wrinkling, cavitation, and distortion occur during the SPF process and need to be addressed (Cappetti et al., 2010; Chatterjee & Mukhopadhyay, 2018; Gillo Giuliano, 2011; Lee, Tang, & Chu, 2016; Luo, Luckey, Friedman, & Peng, 2008; Majidi et al., 2018b, 2019). The impact of these defects become more important when working with large size parts. The SPF process is generally carried out using high temperature presses under isothermal or near isothermal conditions with the SPF die being at the same temperature as the workpiece. In order to form the part, inert gas or air is blown from orifices within the die to deform the sheet material to its final shape. Once the forming process is completed, the part is ejected and a carrier brings the part outside of the press.

The cooling stage is characterized with significant transitional and unsteady heat transfer and mechanical conditions. Specifically, immediately after the end of the forming process, and just before the ejection, the press opens up and cold air comes into contact with the part which is still at high temperature. During the ejection phase, when the part is pushed on the surface of the cold carrier, the upper surface of the die is still at high temperature. During the transport phase to the outside of the press, the part is gradually exposed to the cooling media and

therefore while some sections are still inside the press, other sections are in the open space. Finally, depending on the cooling mode, the part could be cooled from above or below in symmetrical or asymmetrical conditions. Fig. 4-1 shows a schematic view of different stages of the cooling process of a SPF part from the ejection stage until the final cooling. During the cooling process, different heat transfer modes take place, including natural/forced convection, radiation, and conduction and create very dynamic thermal patterns. Such transient thermal conditions result in distortions of the part, which could become unacceptable and require part rework or even rejection.

Fig. 4.1 shows a schematic view of cooling stage of a SPF process including die opening, part loading on carrier, and part exiting.

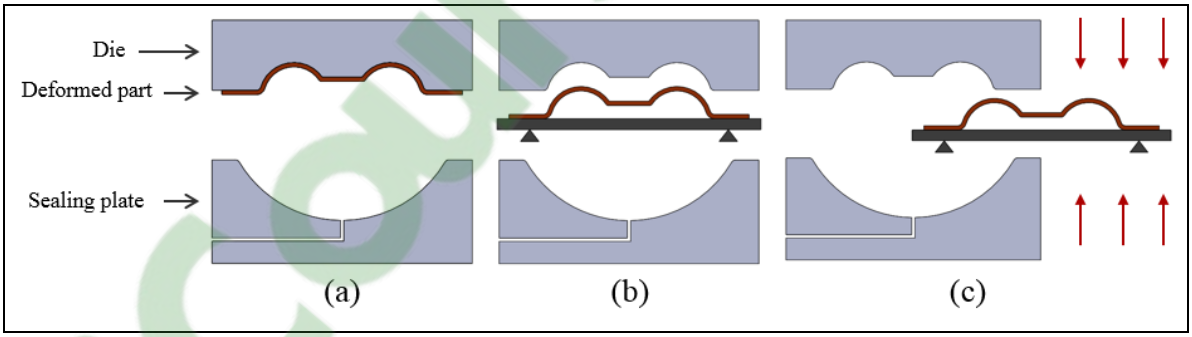

Figure 4-1 The schematic view of a cooling process, a) Die opening, b) Part loading on carrier, c) Part exiting

While a large number of studies are available on the SPF material characterization or forming process simulation (Carrino et al., 2003; Lin, 2003; Mikhaylovskaya et al., 2017; Mosleh et al., 2019; Ridley et al., 2005; Yasmeen et al., 2019) very little data is available on the other aspects of the SPF process, such as lubrication, heating system, etc. (Gao, Lours, & Bernhart, 2005; Mauduit et al., 2017; Sorgente et al., 2016). The occurrence of distortion in different manufacturing processes such as welding, quenching, and machining is very well known and a large number of publications could be found on the analysis, prediction, and control of this

phenomenon (S Bikass et al., 2012; Da Silva et al., 2012; Deng & Murakawa, 2008); however, as mentioned above, very few or no data is available, at least in the open literature, on its occurrence during the SPF process.

The cooling process of a SPF part is mostly done in ambient air with or without cooling media. If used, the cooling media is cooling fans, which is the case of gas cooling. Gas cooling /quenching is a technique that is usually performed in chambers where it is possible to control the flow and pressure of the gas (Lior, 2004). Consequently, there is more control on the cooling and distortion during quenching of a part. As the cooling process in SPF is usually performed in ambient air, there is no specific control on the flow distribution over the part, which further complicates the analysis. The present work was carried out with the objective to experimentally study the influence of different cooling strategies on the distortion of a large size component made of a thin sheet high strength aluminum alloy. Particular attention was paid to the initial temperature distribution of the cooled part. As the temperature variation is one of the most important parameters that affects the distortion during the cooling process, its distribution will have a significant impact on the overall distortion, particularly, in thin and usually large size parts.

In this regard, four industrial size SPF parts were instrumented by thermocouples (TCs) and temperature evolution during the cooling stage of the process were recorded. After the experiments, the parts were completely scanned using a 3D scanner camera and the scanned models were compared with the CAD model of the part. Then the influence of the cooling conditions, Heat Transfer Coefficient (HTC) and temperature variation on the extent of the distortion were analyzed and their impact quantified.

4.2 Experimental procedure and methods

Fig. 4.2 depicts the schematic model of the investigated part. The part was made of a SPF grade 5083 aluminum alloy with the dimensions of 1.91 m×1.44 m×0.0024 m. The physical properties, obtained from the literature, are provided in Table 4.1.

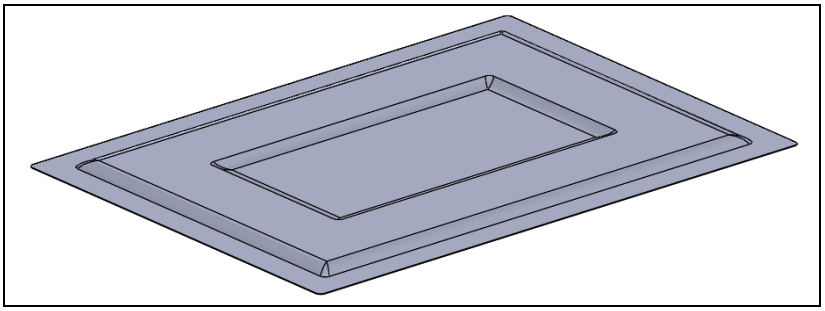

Figure 4-2 The schematic model of the investigated SPF part

Table 4-1 Physical properties of the material

	Thermal conductivity (k) (W/m ºC) (Summers et al., 2015)	Specific heat (C_p) (J/kg ºC) (Summers et al., 2015)	Density (ρ) (kg/m³) (Totten & MacKenzie, 2003)
20 ºC	125	920	2670
100 ºC	135	930	-
200 ºC	145	960	-
300 ºC	155	1010	-
400 ºC	165	1050	-
500 ºC	170	1100	-

For studying the cooling stage, the part was divided into 9 equal zones and a K type thermocouple was attached at the center of each zone. For the purpose of HTC evaluation, the instantaneous temperature within each zone was assumed uniform and the average value was used to obtain the average HTC for the entire part. Fig. 4.3 illustrates a schematic view of the location of the TCs and the 9 zones.

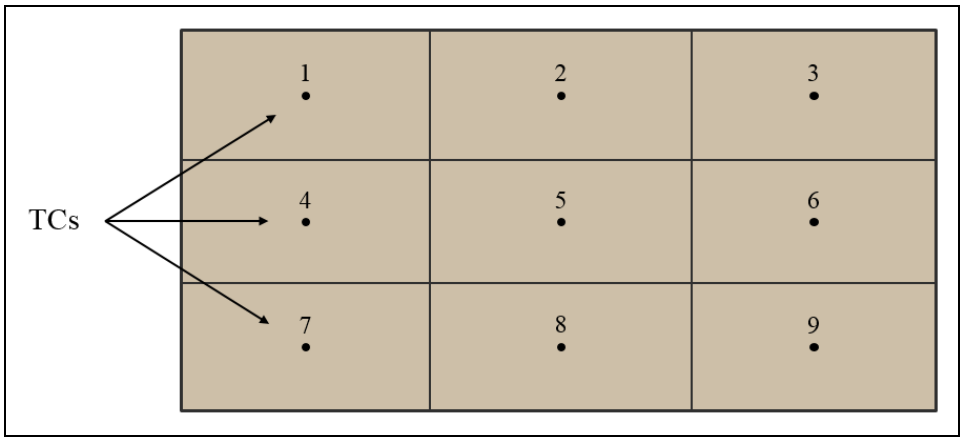

Figure 4-3 The subdivision of the part in 9 zones and the location of the thermocouples.

In order to determine, the most realistically possible, the actual cooling conditions, a full size part and an actual production press was used for the experiments. For each experiment, the part was placed inside the SPF die until its temperature reached the target temperature (≈470 ºC). Then, the SPF die was opened and the carrier moved into the die to carry the part to the outside of the die where a set of blowing fans were used to cool down the part. Temperature evolution during all the experiments was recorded using a 40-channel data logger. The above procedure was repeated four times, corresponding to the different cooling conditions, as detailed in Table 4.2.

In the first experiment, the upper cooling fans located at about 100 cm distance, were active. In the second experiment, in order to examine the effect of the distance from the cooling fans on the distortion of the part, while keeping all other conditions unchanged, the distance between the part and the cooling fans was decreased to about 30 cm. The third experiment was

performed to investigate the effect of the uniformity of the HTC on the distortion. In this case, the SPFed part was cooled without active fans during the cooling process and the part was exposed to a completely natural convection condition. In the fourth experiment, the influence of the initial temperature distribution was investigated. To this end, the initial temperature of one side of the part where TCs 1 to 3 were located, was increased by about 20 ºC, while other experimental conditions were kept similar to experiment number 1. The experimental conditions are summarised in Table 4.2 and Fig. 4.4 shows a photo of the SPF part under the cooling fans. It must be noted that all the fans were identical and the same fan power was used during all the experiments.

Table 4-2 Conditions of the performed experiments

Experiments	**Condition (Distance/fans)**	**Initial temperature distribution (ºC)**								
1	100 cm Active fans	TC1 446	TC2 450	TC3 449	TC4 465	TC5 469	TC6 467	TC7 454	TC8 454	TC9 452
2	30 cm Active fans	TC1 448	TC2 453	TC3 454	TC4 468	TC5 474	TC6 470	TC7 448	TC8 454	TC9 451
3	Inactive fans	TC1 446	TC2 453	TC3 453	TC4 467	TC5 472	TC6 467	TC7 452	TC8 452	TC9 448
4	100 cm Active fans	TC1 467	TC2 468	TC3 467	TC4 472	TC5 472	TC6 473	TC7 450	TC8 453	TC9 455

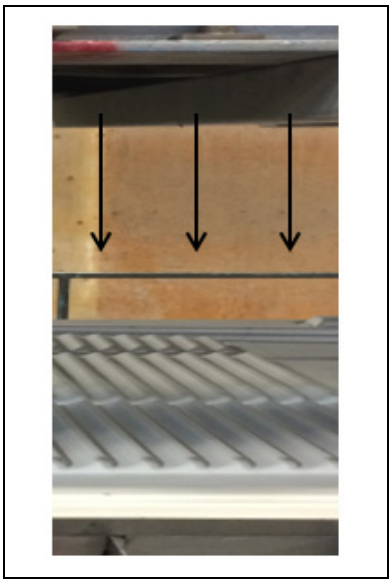

Figure 4-4 The SPF part
under the cooling fans

As indicated in Table 4.2, in experiment 4, TCs are showing more uniform temperature distribution in comparison with the other experiments. In experiments 1, 2 and 3 the temperature of the lateral TCs (1, 2, 3, 7, 8 and 9) are almost the same with an average of 18 ºC lower than that of the central TCs (4, 5 and 6). In contrast, in experiment 4, the temperature of the central (4, 5 and 6) and the upper side (1, 2 and 3) TCs are showing values close to each other and the lower side TCs (7, 8 and 9) have the same values as the other experiments.

After completion of the experiments, the SPF parts were scanned with a 3D scanner camera and the scanned part models were compared with the CAD model of the part using the metrology software PolyWorks and the corresponding distortions were determined.

4.3 HTC calculation

In order to have an overall comparison between the HTC values directly measured from the experiments, the average temperature evolution of each experiment during the entire cooling process was considered and based on the experimental temperature evolution curves, the HTC

values were calculated, in agreement with other reports in the literature (Liščić, 2016; Xiao et al., 2011; Zhang et al., 2013).

For the calculation of the HTC, determining the Biot number is important. If the Biot number is less than 0.1, then the internal conduction within the part could be ignored (Ya, Ghajar, & Ma, 2015). The Biot number is expressed as:

$$Bi = \frac{hL}{k} \tag{4.1}$$

Where k is the heat conduction coefficient (W/m ºC), h is the heat convection coefficient (W/m^2 ºC) and L is the characteristic length (m). Considering the dimensions of the investigated part, L is equal to 0.0024 and the average thermal conductivity (Table 4.1) was estimated to be 150. According to the air cooling condition the average h value is estimated to not be more than several hundreds.

Based on the above values, the Biot number for the considered SPF part was estimated to be less than 0.1. Therefore the internal conduction could be ignored.

On this basis, the h value over a time interval (t_2-t_1) could be obtained from equation (4.2).

$$h = \frac{\rho v c (T_2 - T_1)}{S(T_s - T_\infty)(t_2 - t_1)} \tag{4.2}$$

Where ρ is the density (kg/m³), v is the volume (m³), c is the specific heat (J/kg ºC), T_1 and T_2 (ºC) are the temperatures at times t_1 and t_2 (S), respectively, T_s is the surface temperature (ºC), T_∞ is the ambient temperature (ºC), h is the heat convection coefficient (W/m² ºC), and S is the surface area (m^2). A five seconds time interval (i.e. t_2-t_1=5s) was considered and the average h value was calculated accordingly, as will be discussed below.

4.4 Results and discussion

4.4.1 Temperature evolution

Fig. 4.5 displays the temperature evolution of the SPF part during the cooling experiments for the 9 zones of each part. As it can be seen, the maximum temperature difference during the process occurs in experiment 2, which was exposed to the most severe HTC. The maximum temperature differences in the experiments 1, 2, 3, and 4, are 50 ºC, 76 ºC, 16 ºC, and 58 ºC respectively. The minimum value is for experiment 3 during which the part was cooled in a natural convection mode. Experiments 1 and 4 show a similar pattern of cooling. The only difference between the two experiments was the initial temperature distribution which was more uniform in experiment 4. The longest cooling time corresponds to experiment 3, which was expected as it had the least HTC value among the experiments. However, the most uniform temperature evolution during the cooling process corresponds to this experiment because it has also the most uniform HTC pattern.

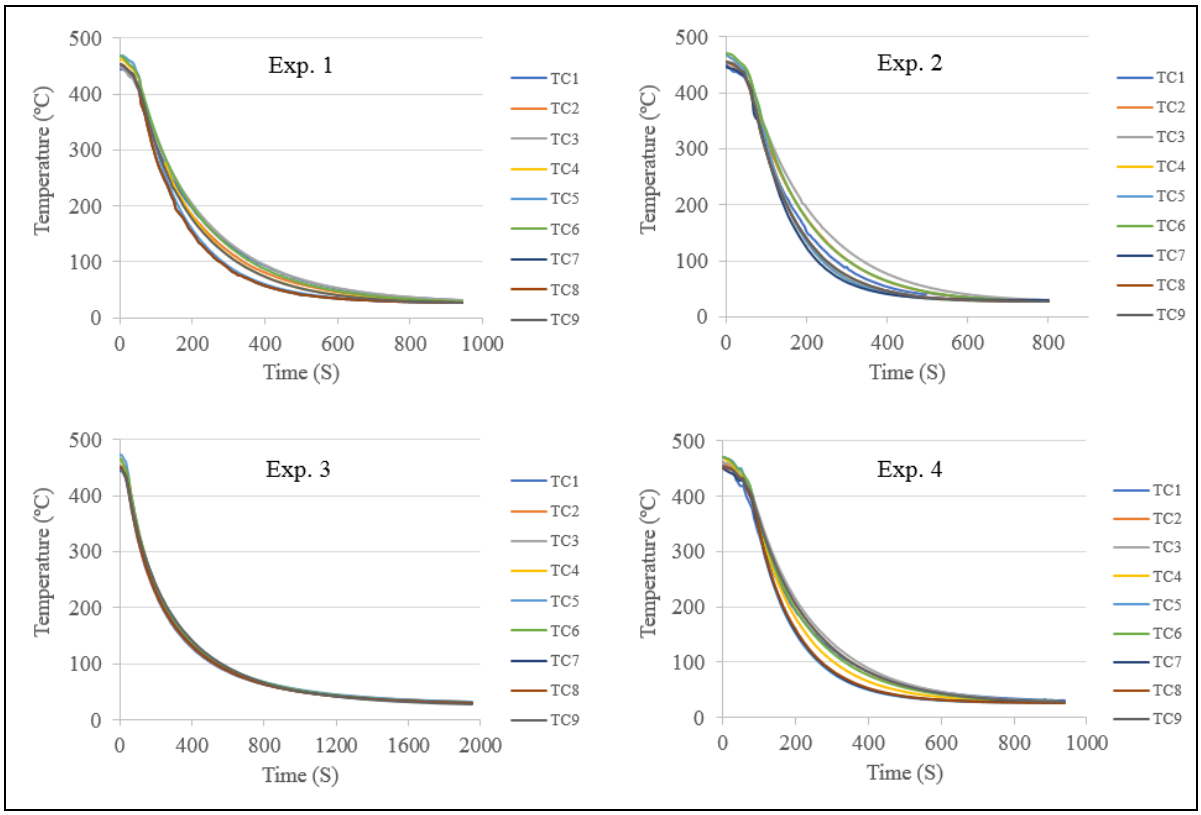

Figure 4-5 Temperature evolution of the SPF part during the cooling stage

4.4.2 HTC evolution

Fig. 4.6 shows the average HTC calculated during the cooling process for each of the four cooling conditions. It must be noted for the purpose of the calculations, the average temperature variations of the 9 TCs were considered and based on that, the average HTC over the whole part was calculated.

The results indicate that the HTCs reach a maximum value at the early stage of the process (when the part is exposed to the blowing fans) and then gradually take a descending trend until the end of the process.

Since experiment 3 was done by inactive fans, it represents the maximum duration of the cooling process while experiment 2 represents the minimum duration, as it was done by active fans and the closest distance from the cooling fans.

A similar comparison can be made between experiments 1 and 2 where it can be seen that by decreasing the distance between the cooling fans and the part, about 20 % gain in average HTC is achieved, which results in 15 % reduction of the cooling duration and 50 % increment of maximum temperature difference during the process. It is also interesting to note that while the cooling time in experiment 3 is twice that of experiment 1, its HTC only shows a 55 % reduction. In experiment 4, the initial temperature distribution is more uniform than that of experiment 1 but the other conditions are the same. Comparison of the results reveals that the cooling time, temperature variations during the cooling, and HTC evolutions are very similar. This indicates that the initial temperature distribution has a little impact on the above-mentioned variables.

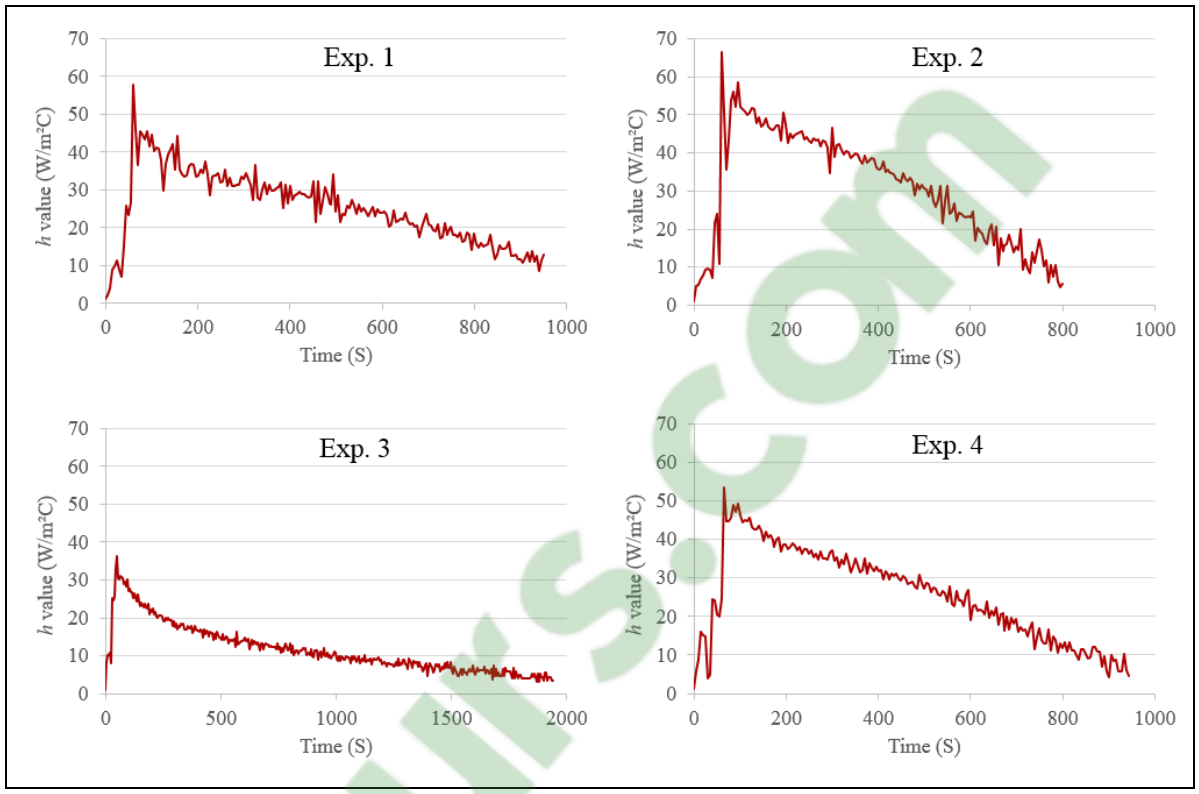

Figure 4-6 The average of the HTC evolution during the cooling stage

4.4.3 Influence of cooling pattern on the distortion

After completion of the experiments, the SPF parts were scanned with a 3D scanner camera and the model files of the scanned parts were compared with the CAD model. Figures 4.7, 4.8, 4.9, and 4.10 show the comparison of the scanned models and the CAD model for the four experimental conditions. It must be mentioned that all units in the color bars are in mm. In all cases, there was no specific reference and the "best fit" option in the metrology software PolyWorks was selected for the comparisons. In the comparison process, the 'best fit' method automatically aligns the two parts and the deviation report could be made in a color map, as shown in the figures.

Fig. 4.7 depicts comparison of the scanned part with the CAD model for experiment 1 where the distance of the part with the cooling fans was 100 cm and the cooling fans were active. The standard deviation between the scanned results and the CAD model was 9.4 mm for this case while this value was 10.7 mm for experiment 2, as reported in Fig 4.8. The result in experiment 2, where the distance of the part from the cooling fans was 30 cm indicates that reducing the fan-part distance and thereby increasing the cooling rate does not necessarily affect the distortion. In experiment 3, the cooling process was done in a natural convection mode and comparison of the final product with the CAD model is illustrated in Fig. 4.9 where a 12.7 mm standard deviation was obtained. As shown in Fig. 4.10, the smallest distortion of 6.7 mm was achieved with experiment 4 characterized by active fans located at 100 cm from the part and with the most uniform initial temperature distribution.

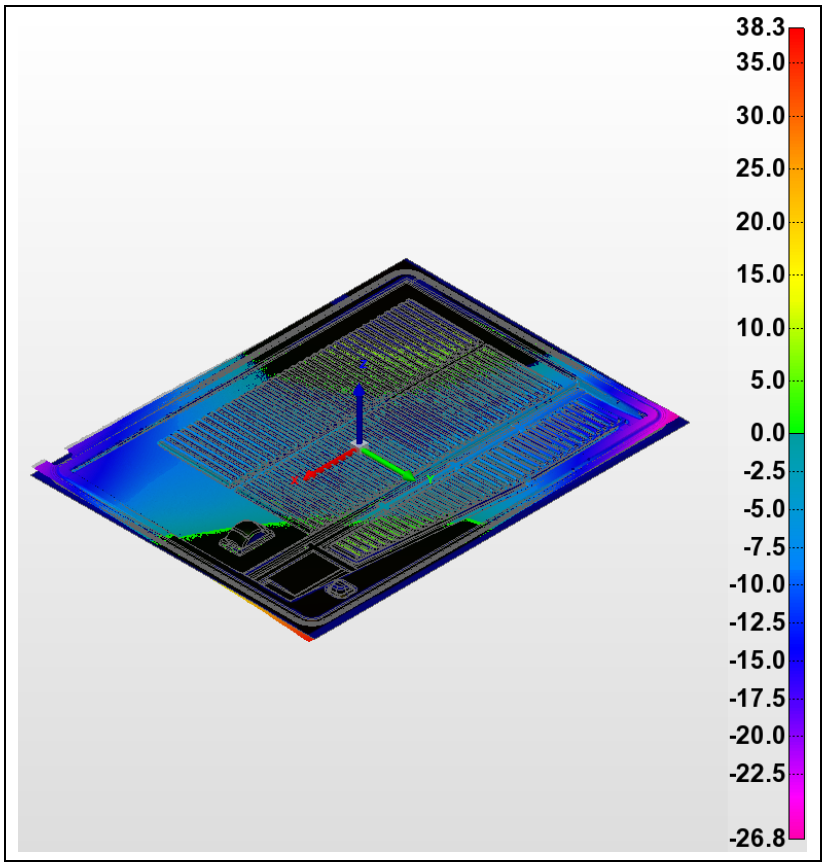

Figure 4-7 Comparison of the SPF part with the CAD model (experiment 1) (All units in the color bars are in mm)

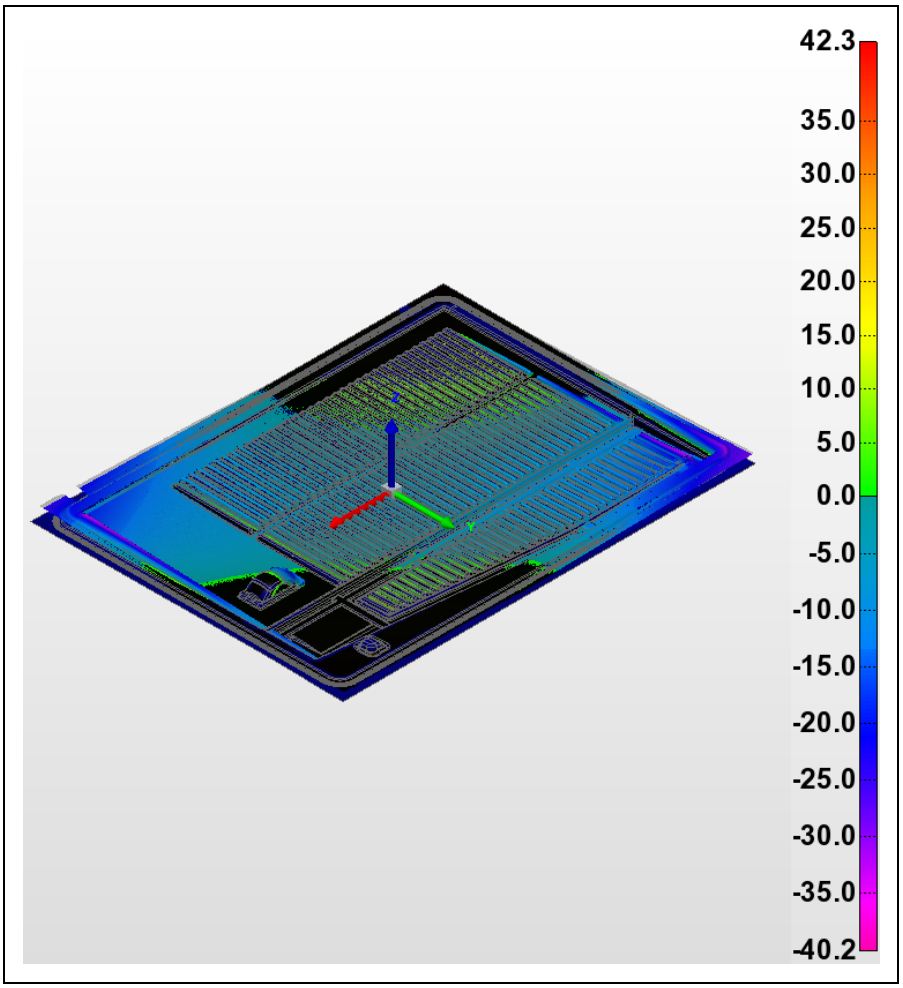

Figure 4-8 Comparison of the SPF part with the CAD model (experiment 2) (All units in the color bars are in mm)

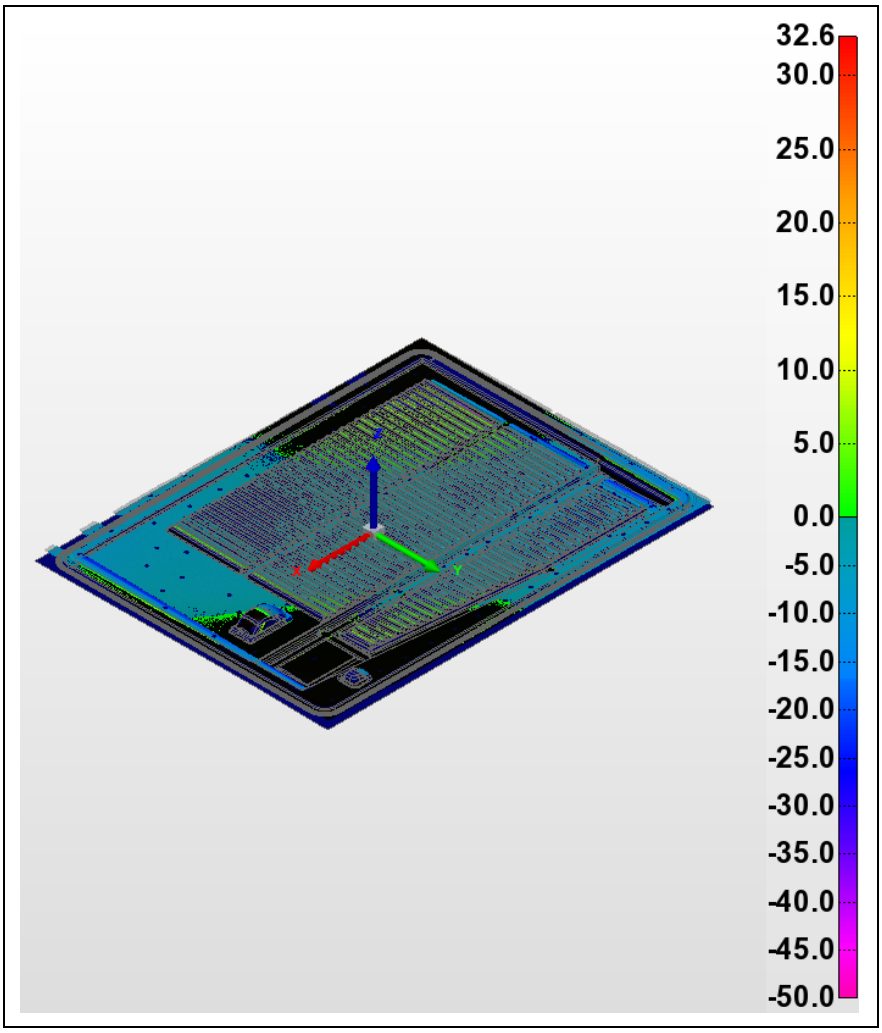

Figure 4-9 Comparison of the SPF part with the CAD model (experiment 3) (All units in the color bars are in mm)

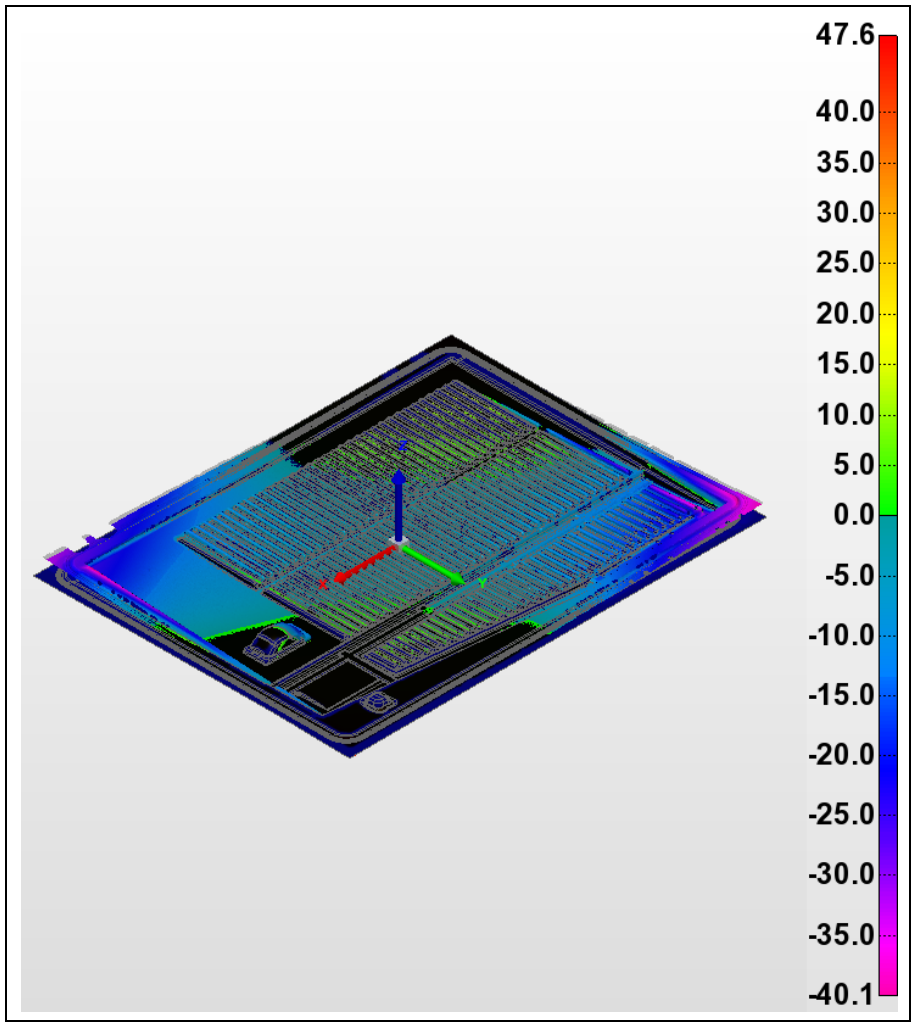

Figure 4-10 Comparison of the SPF part with the CAD model (experiment 4) (All units in the color bars are in mm)

Among all the experiments, most uniform temperature evolutions, with a maximum of 16 ºC difference were observed in experiment 3. These small discrepancies are due to the natural convection mode used for the cooling process. However, it appears that this cooling mode has actually a negative impact on the distortion with the highest value obtained as 12.7 mm. In other words, more uniformity in the HTC, which results in more uniform temperature evolution, did not improve the distortion while increasing the cooling time.

In experiment 4 where the cooling conditions were the same as experiment 1, the distortion was minimal. The HTC value and the temperature evolution in these two experiments were almost the same, and the maximum temperature differences during the process were 50 ºC for experiment 1 and 58 ºC for experiment 4. This observation shows that with keeping the cooling conditions the same, more uniformity in the initial temperature distribution could reduce the distortion while it did not affect the uniformity in the temperature evolution. Therefore, based on the above results it could be said that the uniformity in the initial temperature distribution is more important and more effective parameter than the uniformity in the HTC value on the distortion of the part during the cooling process.

As the initial temperature distribution of the part follows the temperature distribution of the SPF die; therefore, the temperature distribution over the surface of the die should be considered as the source of the temperature distribution over the part. The heat sources in SPF dies are usually heating elements, which can be controlled by controlling systems such as PIDs. Thus, it is possible to minimize temperature discrepancy on the surface of the die through a judicious design of the heating system. In general, obtaining a uniform temperature distribution on the surface of the SPF die is more feasible than that of a uniform air-blowing through the fans. Although uniform air-blowing will result in more uniform temperature evolution during the cooling process but it does not guarantee improvement in the distortion severity. As shown by the results of experiment 4, with more uniformity in the initial temperature distribution, the distortion was improved around 30 % in comparison with experiment 1 while the HTC and temperature discrepancy during the process were almost the same. In contrast, in experiment 3 the temperature discrepancy was considerably improved while there was no improvement in the distortion level.

4.5 Conclusions

In the present study, the influence of initial temperature distribution and cooling conditions on the distortion of a large size thin 5083 aluminum alloy sheet was experimentally studied. Temperature evolution of each part in 9 equally divided zones were recorded during the process

and the distorted parts were scanned with a 3D scanner camera and compared with the CAD model.

The following conclusions can be drawn from the present work:

1. The distance of the part from the cooling fans has a slight effect on the distortion and severity of the HTC value, although it affects the cooling duration.

2. More uniformity in the HTC and temperature evolution during the cooling process did not improve the distortion severity.

3. More uniformity in the initial temperature distribution of the SPF part could reduce the distortion.

4. The generated data will help to develop a systematic database on distortion in SPF process of large size thin components and will also be used as a validation tool for future modeling attempts simulating the entire ejection and cooling process.

CONCLUSION

The focus of this thesis was on the thermal aspect of the SPF/HSBF process and the distortion analysis on the formed part after the cooling step. In this regard, the offline heating process of the SPF/HSBF tool was successfully simulated by ABAQUS and validated through experiment. Further, a thorough experimental and numerical investigation was performed on the cooling step of the process and calculating the HTC was discussed in detail. In the last step, the distortion issue was experimentally taken into account by conducting several experiments. The distorted parts were precisely measured and different cooling strategies were compared. The following summarizes the obtained results in the present thesis.

1) During the offline heating process of the SPF/HSBF tool, the heating rate inside the die is almost the same as the heating rate over the surface.

2) In order to obtain more uniformity in the temperature distribution on the surface of the SPF/HSBF die, considering all heating elements as one zone would result in more uniformity compared with the heating elements divided in two zones.

3) In order to calculate the HTC value during the cooling step, a new approach was used in dividing the SPF part into nine equal zones. This allowed considerably reduction of the calculation time while a good agreement between the numerical and experimental results was obtained.

4) The HTC values during the cooling step were calculated from the original cooling curves and the smoothed ones. The results showed that both approaches present nearly the same level of accuracy.

5) The radiative and conductive heat transfers during the cooling step are both negligible phenomena.

6) During the cooling process, the distance between the part and the cooling fans have a minor impact on the distortion and HTC value.

7) During the cooling step, more uniformity in the HTC and temperature distribution did not show considerable effect (improvement) on the distortion of the part.

8) More uniformity in the initial temperature distribution of the part in the cooling step could reduce the distortion.

RECOMMENDATIONS

As stated in this thesis, the thermal aspect of SPF/HSBF has not been investigated when it comes to the distortion issue which is a major challenge during the production of SPF/HSBF parts. Based on the obtained results during this work, some suggestions for future works are presented as below:

1) In the SPF/HSBF tool, there are heating platens with some insulator material in their structure. As reducing energy consumption and processing time are important parameters that need to be taken into consideration, hence, using more insulator material in the structure of the heating platens could improve and save energy and time during the entire process particularly in the offline heating process. Numerical and experimental analyses could be used to determine the optimum dimensions and amount of insulators to be integrated in the structure of the heating platens.

2) As mentioned, one of the most important parameters during the SPF/HSBF process is uniformity in the temperature distribution over the surface of the die. As demonstrated in this work, heat sources (heating elements in this work) have the main role in this regard. In order to obtain more uniformity in the temperature distribution on the surface of the die, it is suggested to investigate both numerically and experimentally the design and arrangement of heat sources within the tool and the die.

3) Since one of the main challenges in the SPF/HSBF process is the distortion in the formed part, it is recommended to numerically model the distortion during the cooling process. As depicted in this work, measuring the distortion with high accuracy and precision is feasible; hence, with the help of experimental approaches it is possible to validate the numerical model. In this way, the effects of mechanical boundary conditions and also new cooling strategies could be investigated.

LIST OF REFERENCES

Åström, K. J., & Hägglund, T. (1995). *PID controllers: theory, design, and tuning* (Vol. 2): Instrument society of America Research Triangle Park, NC.

Balasubramanian, M., Stalin, B., Ramanathan, K., & Ravichandran, M. (2019). Hot tensile test for determining the material constant on superplastic 5083Al alloy sheet. *Materials Today: Proceedings*.

Bejan, A., & Kraus, A. D. (2003). *Heat transfer handbook* (Vol. 1): John Wiley & Sons.

Bergman, T. L., Incropera, F. P., Lavine, A. S., & DeWitt, D. P. (2011). *Introduction to heat transfer*: John Wiley & Sons.

Bikass, S., Andersson, B., Pilipenko, A., & Langtangen, H. (2012). Simulation of the distortion mechanisms due to non-uniform cooling in the aluminum extrusion process. *International Journal of Thermal Sciences, 52*, 50-58.

Bikass, S., Andersson, B., Pilipenko, A., & Langtangen, H. P. (2012). Simulation of the distortion mechanisms due to non-uniform cooling in the aluminum extrusion process. *International Journal of Thermal Sciences, 52*, 50-58. doi:10.1016/j.ijthermalsci.2011.06.002

Blaise, A., Bourouga, B., Abdulhay, B., & Dessain, C. (2013). *Estimation of the Heat Transfer Conditions in a die Radius during Hot Stamping.* Paper presented at the Key Engineering Materials.

Boissiere, R., Terzi, S., Blandin, J., & Salvo, L. (2008). *Quick-plastic forming: Similarities and differences with super-plastic forming.* Paper presented at the EuroSPF08.

Bruschi, S., Ghiotti, A., & Michieletto, F. (2013). *Hot Tensile Behavior of Superplastic and Commercial AA5083 Sheets at High Temperature and Strain Rate.* Paper presented at the Key Engineering Materials.

Cappetti, N., Garofalo, L., Naddeo, A., Nastasia, M., & Pellegrino, A. (2010). A method for setting variables in Super Plastic Forming process. *Journal of Achievements in Materials and Manufacturing Engineering, 38*(2), 187-194.

Carrino, L., Giuliano, G., & Napolitano, G. (2003). A posteriori optimisation of the forming pressure in superplastic forming processes by the finite element method. *Finite Elements in Analysis and Design, 39*(11), 1083-1093.

Çengel, Y., & Ghajar, A. (2011). *Heat and mass transfer: fundamentals & applications*.

Chandler, H. (1996). *Heat treater's guide: practices and procedures for nonferrous alloys*: ASM international.

Chatterjee, R., & Mukhopadhyay, J. (2018). A Review of Super plastic forming. *Materials Today: Proceedings, 5*(2), 4452-4459.

CROUCHER, T. (2008). Using Glycol to Effectively Control Distortion and Residual Stresses in Heat treated Aluminum Alloys. *Journal of ASTM International*.

Crowe, J., Chen, G., Ferdous, R., Greenwood, D., Grimble, M., Huang, H., . . . Kwong, S. (2005). *PID control: new identification and design methods*: Springer.

Da Silva, A., Pedrosa, T., Gonzalez-Mendez, J., Jiang, X., Cetlin, P., & Altan, T. (2012). Distortion in quenching an AISI 4140 C-ring–Predictions and experiments. *Materials & Design, 42*, 55-61.

Davis, J. R. (1993). *Aluminum and aluminum alloys*: ASM international.

Deng, D., & Murakawa, H. (2008). Prediction of welding distortion and residual stress in a thin plate butt-welded joint. *Computational Materials Science, 43*(2), 353-365.

Faghri, A., Zhang, Y., & Howell, J. R. (2010). *Advanced heat and mass transfer*: Global Digital Press.

Fan, X. B., He, Z. B., & Yuan, S. J. (2012). Deformation behavior of 5A06 aluminum alloy sheet for rapid gas forming at elevated temperature. *Transactions of Nonferrous Metals Society of China, 22*, S389-S394. doi:10.1016/S1003-6326(12)61736-1

Gao, C., Lours, P., & Bernhart, G. (2005). Thermomechanical stress analysis of superplastic forming tools. *Journal of materials processing technology, 169*(2), 281-291.

Giuliano, G. (2011). *Superplastic forming of advanced metallic materials: Methods and applications*: Elsevier.

Giuliano, G., Corrado, A., & Polini, W. (2018). Influence of multiphase forming approach on the thickness uniformity of components from superplastic PbSn60 alloy. *Manufacturing letters, 18*, 16-19.

Guo, Z. X. (2005). *The deformation and processing of structural materials*: Taylor & Francis.

Harrison, N. R., Rubek, V., & Friechnan, P. A. (2013). Warm forming die design, part I: Experimental validation of a novel thermal finite element modeling code. *Journal of Manufacturing Processes, 15*(2), 263-272. doi:10.1016/j.jmapro.2013.01.001

Holman, J. P. (2008). *Heat Transfer (Si Units) Sie*: Tata McGraw-Hill Education.

Hou, L., Cheng, H., Li, J., Li, Z., Shao, B., & Hou, J. (2012). Study on the cooling capacity of different quenchant. *Procedia engineering, 31*, 515-519.

Howell, J. R., Menguc, M. P., & Siegel, R. (2010). *Thermal radiation heat transfer*: CRC press.

http://www.bnzmaterials.com (material producer).

http://www.industries3r.com (material producer)

https://www.verbom.com (supplier of the HSBF die).

Huiping, L., Guoqun, Z., Shanting, N., & Yiguo, L. (2006). Inverse heat conduction analysis of quenching process using finite-element and optimization method. *Finite Elements in Analysis and Design, 42*(12), 1087-1096.

Kaufman, J. G. (2000). *Introduction to aluminum alloys and tempers*: ASM international.

Kessler, O., Irretier, A., Pieper, O., Dolatta, G., Hoffmann, F., & Zoch, H. W. (2006). Distortion Behaviour and Mechanical Properties of AlCu4Mg1 Sheet Components after High-Pressure Gas Quenching in Comparison to Liquid Quenching. *Materialwissenschaft und Werkstofftechnik: Entwicklung, Fertigung, Prüfung, Eigenschaften und Anwendungen technischer Werkstoffe, 37*(1), 110-115.

Kim, H., & Oh, S. (2001). Evaluation of heat transfer coefficient during heat treatment by inverse analysis. *Journal of materials processing technology, 112*(2-3), 157-165.

Kumar, R. R., Ismail, M. Y., Vijayarasi, V. S., & Kumar, V. S. (2019). Effect of grain refinement on superplastic forming of magnesium alloy AZ31 under three different conditions using rectangular die. *Materials Today: Proceedings*.

Lee, S., Tang, J. S., & Chu, C. L. (2016). Prior sheet buckling leading to wrinkling formation in a gas forming a V-trough with wavy bottom. *Journal of Manufacturing Processes, 21*, 101-106.

Li, Z., Zhan, M., Fan, X., Wang, X., Ma, F., & Li, R. (2020). Multi-mode distortion behavior of aluminum alloy thin sheets in immersion quenching. *Journal of materials processing technology, 279*, 116576.

Lin, J. (2003). Selection of material models for predicting necking in superplastic forming. *International Journal of Plasticity, 19*(4), 469-481.

Lior, N. (2004). The cooling process in gas quenching. *Journal of materials processing technology, 155*, 1881-1888.

Liščić, B. (2016). Measurement and Recording of Quenching Intensity in Workshop Conditions Based on Temperature Gradients. *Materials Performance and Characterization, 5*(1), 209-226.

Luo, Y., Luckey, S., Friedman, P., & Peng, Y. (2008). Development of an advanced superplastic forming process utilizing a mechanical pre-forming operation. *International Journal of Machine Tools and Manufacture, 48*(12-13), 1509-1518.

Majidi, O., Jahazi, M., & Bombardier, N. (2018a). *Characterization of mechanical properties and formability of a superplastic Al-Mg alloy.* Paper presented at the Journal of Physics: Conference Series.

Majidi, O., Jahazi, M., & Bombardier, N. (2018b). Finite element simulation of high-speed blow forming of an automotive component. *Metals, 8*(11), 901.

Majidi, O., Jahazi, M., & Bombardier, N. (2019). Prediction of material behavior during biaxial stretching of superplastic 5083 aluminum alloy. *The International Journal of Advanced Manufacturing Technology, 102*(5-8), 2357-2366.

Mauduit, D., Le Fournier, M., Grondin, K., Pottier, T., & Le-Maoult, Y. (2017). Industrial applications of the superplastic forming by using Infra-Red heater. *Procedia engineering, 207*, 1898-1903.

Mikhaylovskaya, A., Mosleh, A., Kotov, A., Kwame, J., Pourcelot, T., Golovin, I., & Portnoy, V. (2017). Superplastic deformation behaviour and microstructure evolution of near-α Ti-Al-Mn alloy. *Materials Science and Engineering: A, 708*, 469-477.

Mis, M., Hall, R., Spence, J., Emekwuru, N., & Kibble, K. (2013). *Numerical study of radiation and temperature phenomena for improved super-plastic sheet metal forming.* Paper presented at the Materials Science Forum.

Mosleh, A., Mikhaylovskaya, A., Kotov, A., & Kwame, J. (2019). Experimental, modelling and simulation of an approach for optimizing the superplastic forming of Ti-6% Al-4% V titanium alloy. *Journal of Manufacturing Processes, 45*, 262-272.

Nazzal, M. A., Khraisheh, M. K., & Darras, B. M. (2004). Finite element modeling and optimization of superplastic forming using variable strain rate approach. *Journal of materials engineering and performance, 13*(6), 691-699.

Padmanabhan, K. A., & Gleiter, H. (2013). *Common mechanism for superplastic deformation in different classes of materials.* Paper presented at the Materials Science Forum.

Padmanabhan, K. A., Vasin, R., & Enikeev, F. (2012). *Superplastic flow: phenomenology and mechanics*: Springer Science & Business Media.

Petiot, A., & Favre, T. (2007). *Tool thermal behavior in SPF environment.* Paper presented at the Materials science forum.

Prantil, V., Callabresi, M., Lathrop, J., Ramaswamy, G., & Lusk, M. (2003). Simulating distortion and residual stresses in carburized thin strips. *J. Eng. Mater. Technol., 125*(2), 116-124.

Priesnitz, K., Sinke, J., & Benedictus, R. (2014). On the simulation of panel distortions due to hot curing adhesives. *International Journal of Solids and Structures, 51*(13), 2470-2478.

Rajan, T., Sharma, C., & Sharma, A. (2011). *Heat treatment: Principles and techniques*: PHI Learning Pvt. Ltd.

Ridley, N., Bate, P., & Zhang, B. (2005). Material modelling data for superplastic forming optimisation. *Materials Science and Engineering: A, 410*, 100-104.

Rollin, M., Velay, V., Penazzi, L., Pottier, T., Sentenac, T., Iranzo-Perez, L., . . . Khelifati, G. (2016). *Thermo-mechanical modeling of distortions promoted during cooling of Ti-6Al-4V part produced by superplastic forming.* Paper presented at the Materials Science Forum.

Shabany, Y. (2009). *Heat transfer: thermal management of electronics*: CRC press.

Sonar, T., Lomte, S., Gogte, C., & Balasubramanian, V. (2018). Minimization of distortion in heat treated AISI D2 tool steel: mechanism and distortion analysis. *Procedia Manufacturing, 20*, 113-118.

Sorgente, D., Palumbo, G., Scintilla, L. D., Brivio, R., Carozzi, G., & Tricarico, L. (2016). *Superplastic forming of a complex shape automotive component with optimized heated tools.* Paper presented at the Materials Science Forum.

Summers, P. T., Chen, Y., Rippe, C. M., Allen, B., Mouritz, A. P., Case, S. W., & Lattimer, B. Y. (2015). Overview of aluminum alloy mechanical properties during and after fires. *Fire Science Reviews, 4*(1), 3.

Tan, M., Liew, K., & Tan, H. (2007). Cavitation and grain growth during superplastic forming. *Journal of Achievements in Materials and Manufacturing Engineering, 24*(1), 307-314.

Tang, J.-S., Fuh, Y.-K., & Lee, S. (2015). Superplastic forming process applied to aero-industrial strakelet: wrinkling, thickness, and microstructure analysis. *The International Journal of Advanced Manufacturing Technology, 77*(5-8), 1513-1523.

Totten, G. E. (2002). *Handbook of residual stress and deformation of steel*: ASM international.

Totten, G. E., & MacKenzie, D. S. (2003). *Handbook of aluminum: vol. 1: physical metallurgy and processes* (Vol. 1): CRC press.

Velay, V., Cutard, T., & Guegan, N. (2008). *Thermal behaviour modelling of superplastic forming tools.* Paper presented at the EuroSPF08.

Velay, V., Cutard, T., & Guegan, N. (2012). Thermal behaviour modelling of superplastic forming tools. *Materialwissenschaft und Werkstofftechnik, 43*(9), 799-804.

Vijayananth, S., Jayaseelan, V., & Kumar, N. M. (2019). High-temperature superplasticity and its deformation mechanism of AA6063/SICp. *Case Studies in Thermal Engineering*, 100479.

Wilson, J. S. (2004). *Sensor technology handbook*: Elsevier.

Xiao, B., Wang, G., Wang, Q., Maniruzzaman, M., Sisson, R. D., & Rong, Y. (2011). An experimental study of heat transfer during forced air convection. *Journal of materials engineering and performance, 20*(7), 1264-1270.

Xu, F. (2006). *Finite element simulation of water cooling process of steel strips on runout table.* University of British Columbia.

Ya, C., Ghajar, A., & Ma, H. (2015). Heat and Mass Transfer Fundamentals & Applications: McGraw-Hill.

Yang, X.-w., Zhu, J.-c., Lai, Z.-h., Yong, L., Dong, H., & Nong, Z.-s. (2013). Finite element analysis of quenching temperature field, residual stress and distortion in A357 aluminum alloy large complicated thin-wall workpieces. *Transactions of Nonferrous Metals Society of China, 23*(6), 1751-1760.

Yasmeen, T., Shao, Z., Zhao, L., Gao, P., Lin, J., & Jiang, J. (2019). Constitutive modeling for the simulation of the superplastic forming of TA15 titanium alloy. *International Journal of Mechanical Sciences, 164*, 105178.

Zhang, L., Feng, X., Li, Z., & Liu, C. (2013). FEM simulation and experimental study on the quenching residual stress of aluminum alloy 2024. *Proceedings of the Institution of Mechanical Engineers, Part B: Journal of Engineering Manufacture, 227*(7), 954-964.

Zhao, L., Yasmeen, T., Gao, P., Wei, S., Bai, Z., Jiang, J., & Lin, J. (2017). Mechanism-based constitutive equations for superplastic forming of TA15 with equiaxed fine grain structure. *Procedia engineering, 207*, 1874-1879.